European Journal of Medicinal Chemistry 132 (2017) 42–62

Contents lists available at ScienceDirect

European Journal of Medicinal Chemistry

journal homepage: http://www.elsevier.com/locate/ejmech

Research paper

Design, synthesis and biological evaluation of novel coumarin-based benzamides as potent histone deacetylase inhibitors and anticancer agents

Tooba Abdizadeh [a, b], Mohammad Reza Kalani [c, d], Khalil Abnous [e], Zahra Tayarani-Najaran [f], Bibi Zahra Khashyarmanesh [b], Rahman Abdizadeh [g], Razieh Ghodsi [a, b, **], Farzin Hadizadeh [a, b, *]

[a] Biotechnology Research Center, Mashhad University of Medical Sciences, Mashhad, Iran
[b] Department of Medicinal Chemistry, School of Pharmacy, Mashhad University of Medical Sciences, Mashhad, Iran
[c] School of Cell and Molecular Biology, University of Illinois at Urbana-Champaign, Urbana, United States
[d] Department of Molecular Medicine, Golestan University of Medical Sciences, Golestan, Iran
[e] Pharmaceutical Research Center, Mashhad University of Medical Sciences, Mashhad, Iran
[f] Department of Pharmacodynamics and Toxicology, School of Pharmacy, Mashhad University of Medical Sciences, Mashhad, Iran
[g] Department of Medical Parasitology and Mycology, Faculty of Medicine, Shahrekord University of Medical Sciences, Shahrekord, Iran

ARTICLE INFO

Article history:
Received 29 January 2017
Received in revised form
6 March 2017
Accepted 14 March 2017
Available online 18 March 2017

Keywords:
Histone deacetylase inhibitors
Coumarin
2-AminoBenzamide
Docking
Molecular dynamics

ABSTRACT

Histone deacetylases (HDACs) are attractive therapeutic targets for the treatment of cancer and other diseases. It has four classes (I-IV), among them especially class I isozyme are involved in promoting tumor cells proliferation, angiogenesis, differentiation, invasion and metastasis and also viable targets for cancer therapeutics. A novel series of coumarin-based benzamides was designed and synthesized as HDAC inhibitors. The cytotoxic activity of the synthesized compounds (**8a**-**u**) was evaluated against six human cancer cell lines including HCT116, A2780, MCF7, PC3, HL60 and A549 and a single normal cell line (Huvec). We evaluated their inhibitory activities against pan HDAC and HDAC1 isoform. Four compounds (**8f**, **8q**, **8r** and **8u**) showed significant cytotoxicity with IC_{50} in the range of 0.53–57.59 μM on cancer cells and potent pan-HDAC inhibitory activity (consists of HDAC isoenzymes) (IC_{50} = 0.80 −14.81 μM) and HDAC1 inhibitory activity (IC_{50} = 0.47–0.87 μM and also, had no effect on Huvec (human normal cell line) viability (IC_{50} > 100 μM). Among them, **8u** displayed a higher potency for HDAC1 inhibition with IC_{50} value of 0.47 ± 0.02 μM near equal to the reference drug Entinostat (IC_{50} = 0.41 ± 0.06 μM). Molecular docking studies and Molecular dynamics simulation of compound **8a** displayed possible mode of interaction between this compound and HDAC1enzyme.

1. Introduction

Cancer, the uncontrolled, rapid and pathological proliferation of abnormal cells, is one of the most life-threating diseases and cause of death worldwide. Cancer causes about 550,000 deaths a year and is second leading cause of death in the world next to heart diseases [1,2]. The numerous drugs have been used for the cancer treatment but have severe side effects. Consequently; increasing interest has been devoted to the design and discovery of more effective anticancer agents with promising activity and high therapeutic index in current medicinal chemistry. Over the recent years, a great many of important targets such as the histone deacetylase (HDAC) has been considered for anticancer therapies. HDACs and histone acetyl transferases (HATs) are crucial post-translational modification and play a pivotal role in the epigenetic regulation of gene expression through chromatin modification [3–6]. Histone acetyl transferase

Abbreviations: HDAC, Histone Deacetylases; HATs, Histone Acetyl Transferases; HSP 90, Heat Shock Protein 90; SAHA, suberoylanilide hydroxamic acid; TSA, Trichostatin A; ZBG, Zinc Binding Group; CU, Connect Unit; MD, Molecular Dynamics; CDI, *N*, *N*'-Carbonyldiimidazole.

* Corresponding author. Biotechnology Research Center, Mashhad University of Medical Sciences, Mashhad, Iran.
** Corresponding author. Department of Medicinal Chemistry, School of Pharmacy Mashhad University of Medical Sciences, Mashhad, Iran.
E-mail addresses: ghodsir@mums.ac.ir (R. Ghodsi), hadizadehf@mums.ac.ir (F. Hadizadeh).

http://dx.doi.org/10.1016/j.ejmech.2017.03.024
0223-5234/

(HATs) catalyzes acetylation of positive charged lysine residues and leads to the relaxation of chromatin and activates transcription [7]. Inversely, histone deacetylase (HDAC) catalyze the removal of acetyl groups of the ε-amino of lysine residues on core histone and other cellular proteins (e.g. HSP 90, tubulin), resulting in chromatin condensation and transcriptional repression [8,9].

HDACs have an important effect on gene transcription, the cell cycle, differentiation, apoptosis and tumourigenesis. Therefore, HDACs have been become as prominent therapeutic target for a broad range of human disorder such as cancer [10]. There are 18 isoforms of human HDAC, divided into four main classes based on their homology to yeast models, subcellular localization and enzymatic activities [11].

HDACI (HDAC 1, 2, 3 and 8), class IIa (HDAC 4, 5, 7 and 9), class IIb (HDAC 6 and 10) and class IV (HDAC11) are zinc-dependent enzymes, whereas class III HDACs (sirtuins 1–7) are NAD^+ dependent enzymes [12–14]. Class I HDACs are homologous to yeast Rpd3 and are predominantly located in the nucleus (350–500 amino acids in length) and class II HDACs have sequence homology to yeast Hda2 and shuttle between the cytoplasm and nucleus (about 1000 amino acids in length) [15–17]. Class III are homologues of the yeast Sir2 and class IV shows the characteristics of both class I and II HDACs [18].

Zn^{2+}-dependent HDACs, especially class I isozymes are involved in promoting tumor cells proliferation, angiogenesis, differentiation, invasion and metastasis and also viable targets for cancer therapeutics [19]. Among the class I HDAC isoforms, HDAC1 has a key role in cancer [20] and overexpressed in prostate, ovarian, breast, colon, leukemia and pancreas cancers [21].

HDAC inhibitors (HDACIs) are categorized into four classes according to their chemical structure in clinical studies: hydroxamic acids (Trichostatine A (TSA)) [22], (Vorinostat (SAHA)) [23], (Panobinostat (LBH-589)) [24], (Belinostat (PXD-101)) [25], benzamides ((Entinostat (MS-275)) [26], (Mocetinostat (MGCD-0103)) [27,28], (Chidamide (CS-055)) [29], (Tacedinaline (CI-994)) [30], short-chain fatty acids (valproic acid) [31,32] and depsipeptides (Romidepsin (FK-228)) [33]. Up to now, five HDACIs Vorinostat, Romidepsin, Belinostat, Chidamide and Panobinostat approved by FDA for the treatment of lymphoma or myeloma [34]. The structures of several approved and clinical HDACI are shown in Fig. 1.

Development of selective isotope HDACIs is a significant way for prevention of the side effects of HDACIs. Many hydroxamate HDACIs do not exert excellent selectivity toward a specific isoform, while 2-aminobenzamides exert some isoform selectivity such as Entinostat and Mocetinostat are relatively unique in inhibiting HDAC 1, 2 and 3 [35].

Despite the huge structural diversity, the HDACIs generally have a general pharmacophore model [36]: zinc binding group (ZBG) such as hydroxamic acid and 2-amino benzamide which interacting to Zn^{2+} at the bottom of active site and a requirement for the possession of HDAC inhibitory activity, a hydrophobic linker occupying the narrow tunnel of HDACs and connect the ZBG and the cap group, a polar connect unit (CU) that connecting cap group and linker, a surface recognition group (cap), a hydrophobic and aromatic or heteroaromatic group, is essential for recognizing and interacting with residues on the rim of active site of HDACs [37]. A cap group determines the potency, stability, bioavailability and efficacy of the compounds [11,38]. Coumarins (2H-1-benzopyran-2-one or 2H-chromen-2-one), an important bicyclic heterocycle as a part of flavonoid group of plant metabolite, are a wide class of natural and synthetic compounds that show anticancer [39], *anti*-HIV [40], anti-Alzheimer [41],antimicrobial [42],antioxidant [43] and antiviral [44] activities. Coumarin and its derivatives have rare nephrotoxicity, hepatotoxicity, cardio toxicity, dermal toxicity and other side effect [45].

In the present study some new coumarin-based benzamides have been designed and synthesized as HDAC inhibitors, as an attempt to check if the replacement of the benzyl carbamate moiety of Entinostat or (E)-3-(pyridin-3-yl)acrylamide moiety of Chidamide with the coumarin carboxamide are bioisosteric. The rationale for the design of these compounds was depicted in Fig. 2. We selected Entinostat and chidamide as the lead compounds and our design strategy for novel HDAC inhibitors was based on the common pharmacophore model of HDACs.

The synthesized compounds were evaluated for their cytotoxic activity against six different cancer cell lines including HCT116 (human colon cancer cells), A2780 (human ovarian cancer cells), MCF7 (human breast cancer cells), PC3 (human prostate cancer cells), HL60 (Human promyelocytic leukemia cells) and A549 (adenocarcinoma human alveolar basal epithelial cells) and normal Huvec cell line (Human Umbilical Vein Endothelial Cells). We evaluated their inhibitory activities of pan HDAC and HDAC1 isoform. The structure activity relationships (SAR) study performed on the cap moiety by investigating the electronic effects of the alkoxy or benzyloxy ring with various substituents. Docking and molecular dynamics (MD) simulation were performed for further investigating interaction of compounds with HDAC1.

2. Results and discussion

2.1. Chemistry

The synthetic routes to target compounds containing the coumarin ring were illustrated in Schemes 1–3. Appropriately, ethyl coumarin-3-carboxylates **3a-e** were synthesized through the knoevenagel condensation of salicylaldehydes **1a-e** with diethyl malonate in the presence of catalytic amount of piperidine in ethanol. Then, O-alkylation or *O*-benzylation of the 7-hydroxy derivative **3e** with alkyl halides or benzyl halides was done in DMF in the presence of potassium carbonate. The ethyl esters **3a-v** were hydrolyzed with aqueous solution of sodium hydroxide to the corresponding coumarin-3-carboxylic acids **4a-u** (Scheme 1) [46].

The condensation of the carboxylic acids **4a-u** with 4-(aminomethyl) benzoic acid using *N*, *N*'-carbonyldiimidazole (CDI) and trifluoroacetic acid (TFA) in dry THF at room temperature led to the formation of compounds **6a-u** (Scheme 2) [30].

Finally, compounds **6a-u** were converted into imidazole intermediate with CDI at 55–60 °C in dry THF, then reacted in situ with *o*-phenylene diamine in the presence of TFA at room temperature to obtain the target benzamide analogs **8a-u** as depicted in Scheme 3. The chemical structures of final compounds were characterized by ^1H NMR, ^{13}C NMR, elemental analysis, IR and MS spectroscopy.

2.2. Biological evaluation

2.2.1. In vitro anticancer activity

As depicted in Tables 1–3, the antiproliferative activity of the target compounds (**8a-u**) was evaluated against seven human cell lines including HCT116, A2780, MCF7, A549, PC3, HL60 and Huvec by 3-(4,5-dimethylthylthiazol-2-yl)-2,5-diphenyltetrazolium bromide (MTT) assay using Entinostat as the positive control. Most of the target compounds showed significant anti proliferative activity with the IC_{50} values in micromolar range (0.27–80 μM) over all cell lines. Compounds **8k** was the most potent compound with IC_{50} values of 8.48, 10.14 and 16.6 μM in MCF7, A2780 and PC3, respectively. This compound also showed superior activity against HCT116, A549 and HL60 cells (IC_{50} = 0.27, 1.69 and 3.14 μM) compared with the reference drug Entinostat (IC_{50} = 2.03, 3.11 and 4.53 μM). Overall, the majority of the synthesized compounds were more potent against cell proliferation in HCT116 and A2780 cell,

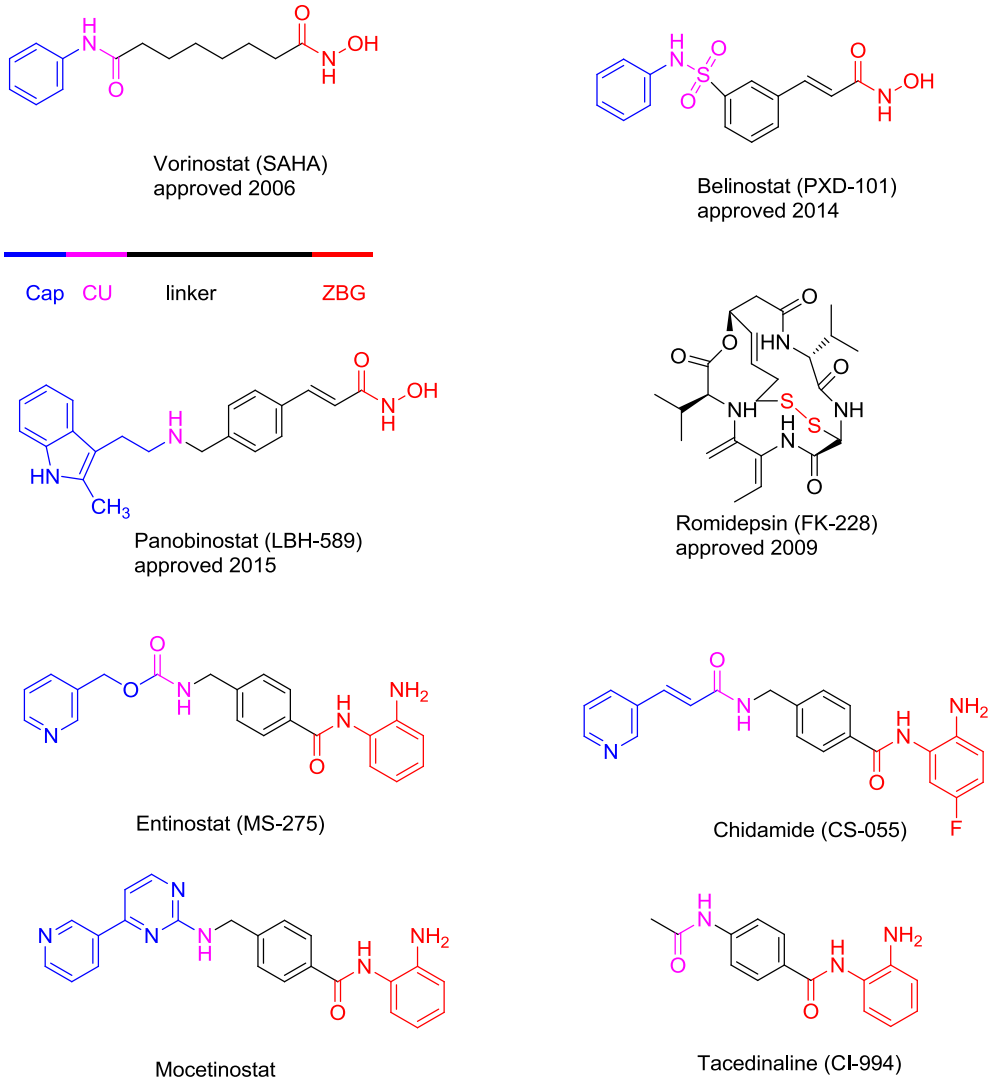

Fig. 1. Pharmacophore model and structures of approved and in clinical trials HDAC inhibitors.

indicating that our compounds exerted their cytotoxic activity with different mechanisms in different tumor cells. Another interesting aspect of the results was that A549 and HL60 cell lines were sensitive to all the coumarin-based derivatives (IC_{50} < 80 μM). Some of the compounds showed promising antiproliferative against PC3 (**8i-k**; **8n-u**) and MCF7 cells (**8e-u**) with IC_{50} < 80 μM.

2.2.2. Cellular HDAC inhibition assay of the target compounds

Since our compounds showed more cytotoxicity effects in human colon cancer HCT116 and ovarian cancer A2780 cell lines in comparison to other cell lines, in vitro pan-HDAC inhibitory activity of the synthesized target compounds **8a-u** were evaluated on these two cell lines in comparison with Entinostat as the reference drug, the results are presented in Table 2.

Since the linker and metal binding moieties of compounds **8a-u** were identical with Entinostat; differences in cellular effects were most likely due to the coumarin portion of the molecules as cap group. In general benzyloxy coumarin derivatives showed stronger HDAC inhibitory activity in comparison to alkoxy coumarin derivatives; this might be because of their more lipophilicity. SAR data showed that the position and the length of alkoxy group have key roles in their HDAC inhibitory and cytotoxicity activities. Compounds possessing methoxy or ethoxy groups on position 7 of coumarin (**8d** and **8e**) showed more cytotoxicity activity than their 8-alkoxy isomers (**8b** and **8c**). Among alkoxy coumarin derivatives, 7-propoxy derivative showed the most HDAC inhibitory and antiproliferative activities in most of cancer cells. Compound **8k** possessing *p*-tolyloxy moiety was the most potent HDAC inhibitor with IC_{50} value of 0.25 and 2.06 μM, in HCT116 and A2780 cell lines respectively. This compound displayed a higher HDAC inhibitory activity (IC_{50} = 1.96 in HCT116) than Entinostat and IC_{50} = 3.15 μM in A2780 cell line). Compounds **8q** and **8u** also exhibited potent HDAC inhibitory activities with IC_{50} values of 0.42, 0.80 μM in HCT116 and 5.41, 4.90 μM in A2780 cancer cells, respectively.

We observed a significant correlation between HDAC inhibition and MTT data (r > 0.8) the same as a previous report [47]. This correlation supported our hypothesis that HDAC inhibition mediates cytotoxicity (Fig. 3.) Small differences between this assay and cytotoxicity values may be attributed to various incubation times used in these tests - 48 h for MTT against 18 h for HDAC inhibition assay.

From the point of view structure activity relationship, compound **8a** as the simplest compound with no substitution on the cap group displayed significant activity against HDAC in both cell

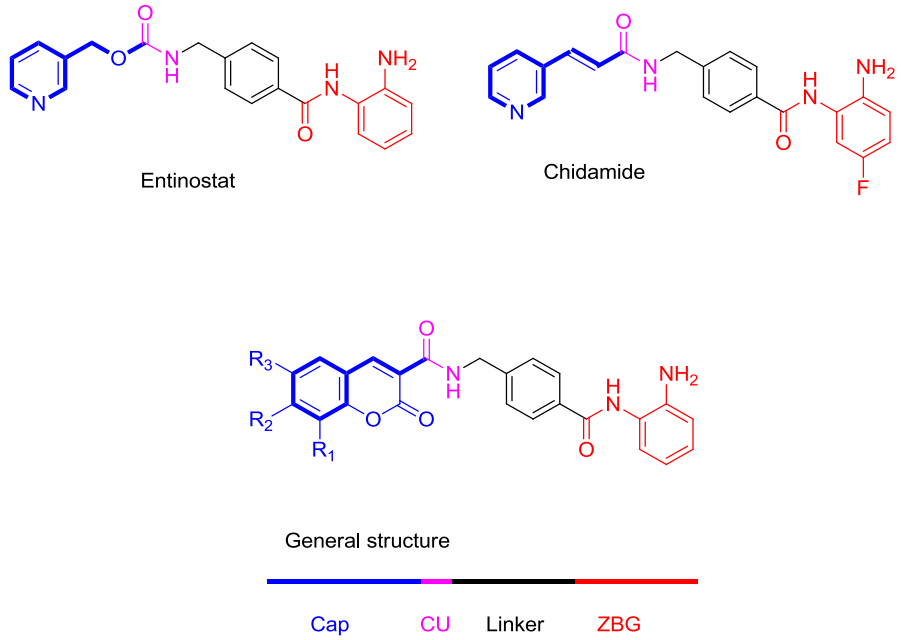

Fig. 2. Chemical structures of known HDAC inhibitors and the structure of our designed compounds.

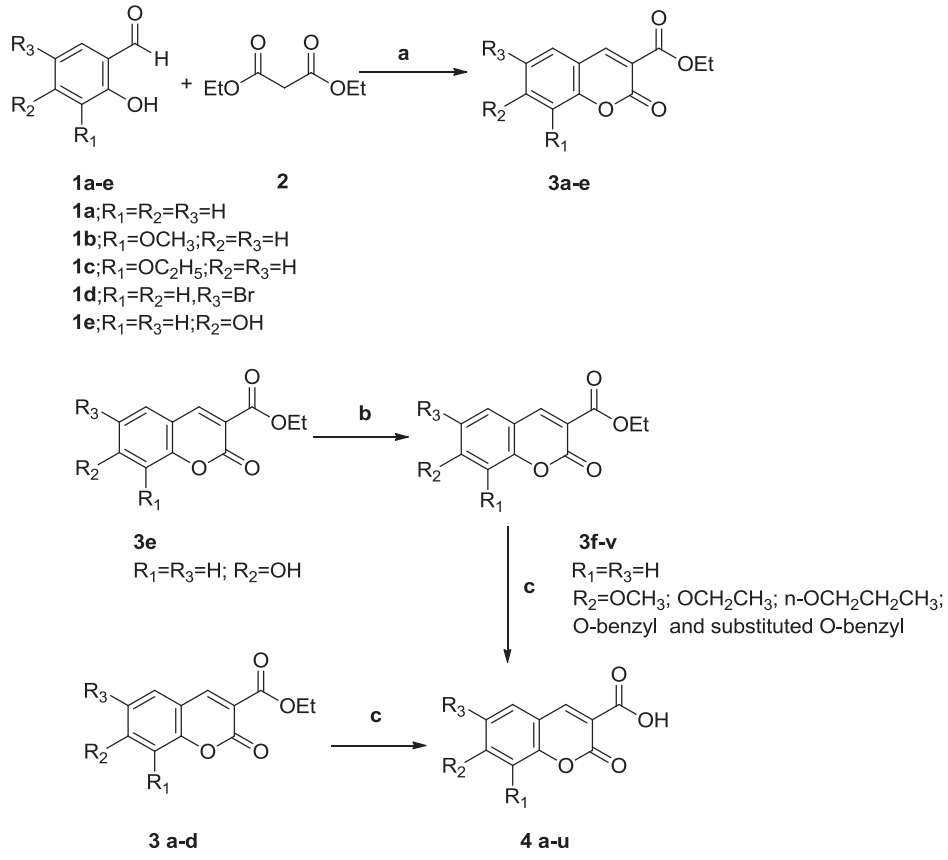

Scheme 1. Reagents and conditions: (a) Piperidine, EtOH, reflux; (b) RX, K_2CO_3, DMF, rt; (C) NaOH (2 N), rt and then HCl (2 N).

lines (11.41 μM in HCT116 and 54.92 μM in A2780). The substitutions at the different positions on the benzene ring of coumarin affected the HDAC inhibition activity. Introduction of 6-bromo substituent on coumarin ring increased inhibitory activity in compound **8g**. Also, the presence of 8-methoxy and 8-ethoxy substitutions showed higher inhibitory than parent compound **8a**. 7-*O*-alkyl or O-benzyl derivatives could increase the activity. In the 7-alkoxy derivatives **8d-f**, 7-propoxy coumarin derivative **8f**

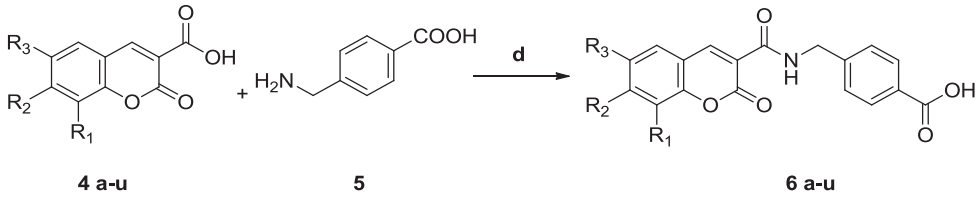

Scheme 2. Reagents and conditions: (d) (i) CDI, THF, rt; (ii) TFA, rt.

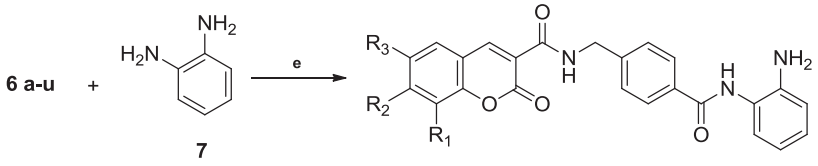

8 a-u

8a: R_1=R_2=R_3=H
8b: R_1=OCH_3; R_2=R_3=H
8c: R_1=OCH_2CH_3; R_2=R_3=H
8d: R_1=R_3=H; R_2=OCH_3
8e: R_1=R_3=H; R_2=OCH_2CH_3
8f: R_1=R_3=H; R_2=$OCH_2CH_2CH_3$
8g: R_1=R_2=H;R_3=Br
8h: R_1=R_3=H; R_2=O-benzyl
8i: R_1=R_3=H; R_2=2-CH_3-benzyloxy
8j: R_1=R_3=H; R_2=3-CH_3-benzyloxy
8k: R_1=R_3=H; R_2=4-CH_3-benzyloxy
8l: R_1=R_3=H; R_2=2-F-benzyloxy
8m: R_1=R_3=H; R_2=3-F-benzyloxy
8n: R_1=R_3=H; R_2=4-F-benzyloxy
8o: R_1=R_3=H; R_2=2-Cl-benzyloxy
8p=R_1=R_3=H; R_2=4-Cl-benzyloxy
8q=R_1=R_3=H; R_2=4-Br-benzyloxy
8r=R_1=R_3=H; R_2=4-OCH_3-benzyloxy
8s=R_1=R_3=H; R_2=2,3-di-Cl-benzyoxy
8t=R_1=R_3=H; R_2=2,4-di-Cl-benzyloxy
8u=R_1=R_3=H; R_2=3,4-di-Cl-benzyloxy

Scheme 3. Reagents and conditions: (e) (i) CDI, THF, reflux; (ii) TFA, rt.

displayed the significant activity with IC_{50} 1.09 and 14.81 μM on cell lines. These results suggested that bulky R groups were beneficial for binding of these molecules to HDAC, which may be related to the hydrophobic effect of the cap groups to penetrate the cell membrane and also enlargement of cap group size facilitated occupation of the active site and thus prevented the substrate from entering to the catalytic center.

The O-benzyl derivative **8h** with IC_{50} values of 2.49 and 12.82 μM in HCT116 and A2780 cell lines respectively was about four times more potent than compound **8a**.

The variety and position of substitutions on benzyl ring of coumarin played important role in inhibitory activity. Potency in the O-benzyl derivatives could be further improved by the introduction of electron-donating or electron-driving substitutions on the benzyl ring of the coumarin. About these substitution, a trend of the inhibition enzymatic values is observed for methyl > methoxy > bromo > Chloro > Fluoro > H. Compounds **8i-k** with *o, m or p*-methyl group on O-benzyl demonstrated significant HDAC inhibition with IC_{50} of 1.40 (*o*-), 1.31 (*m*-), 0.25 μM (*p*-) in HCT116 in comparison with the values of IC_{50} in A2780 (20.84, 10.10 ± 0.59 and 2.06 μM respectively). Compound **8q** with a 7-bromo substituent was the most potent inhibitor between halo-substituted compounds (**8l-q**). This might be due to less electronegativity of bromo in comparison to fluoro, so the π-electron density on the benzyl ring with bromo substituent was a little dense. Thus, the π-π interaction between benzyl and the HDAC active site might be slightly stronger. On the other, an *o*-substituent, in comparison with *para* or *meta* substituent, on the benzyl decreased the HDAC inhibition activity (**8i** vs **8j** and **8k**; **8l** vs. **8m** and **8n**; **8o** vs **8p**). These findings confirmed that position of the substitutions on the O-benzyl group had significant effect on enzyme activity. By comparing IC_{50} values of chloro derivatives, it could be concluded that the introduction of second chloro atom onto the benzyl ring dramatically changed the *anti*-HDAC activity and 3,4-dichloro derivative **8u** with 0.80 and 4.90 μM in HCT116 and A2780 was more potent than 2,3-dichloro **8s** and 2,4-dichloro **8t** derivatives (IC_{50} = 7.66, 38.72 (**8s**) and IC_{50} = 6.32, 27.57 (**8t**)). Also, SAR data suggested that the introduction of the O-benzyl group into C-7 position of coumarin derivatives improved the HDAC inhibition potency than their O-alkyl group. In general, modification of the lipophilic cap group led to increase the inhibitory activity of the target compounds against HDAC.

Direct HDAC1 inhibition assay which will be discussed below, confirmed the latter (Table 3).

ClogP is an important factor in membrane permeability and hence antiproliferative activity. Theoretical logP (Clog P) values (http://www.organic-chemistry.org/prog/peo/) of compounds also were measured. These compounds had ClogP values in range of 2.43–5. (Table 2). In general there is a correlation between ClogP values and HDAC inhibition and MTT data. Compounds with more ClogP values, showed more activity in comparison with those with less ClogP.

2.2.3. HDAC1 inhibition assay of the target compounds

In effort for discovery of anticancer drugs, HDAC1 protein was targeted since it is widely implicated in both transcriptional repression and chromatin remodeling. Thus, the most potent of compounds were selected for HDAC1 inhibition assay which exhibited higher cytotoxic effect and HDAC inhibitory potency (Table 2) and were not toxic to normal cells (IC_{50} > 100 μM).

As shown in Table 3, these compounds inhibited the deacetylase activity of HDAC1 significantly. Compound **8u** inhibited HDAC1 with an IC_{50} value of 0.47 μM and showed near equal effect to Entinostat (IC_{50} = 0.41 μM). Compound **8u** showed more selectivity

Table 1
The in vitro antiproliferative activities (IC_{50} (μM)[a]) of compounds **8a**-**u** and Entinostat against human cancer cell lines.

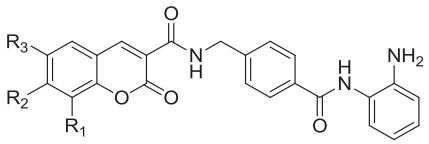

Compound	R_1	R_2	R_3	MCF7	A549	PC3	HL-60
8a	H	H	H	>100	80.81 ± 1.48	>100	76.64 ± 2.87
8b	CH_3O	H	H	>100	76.85 ± 2.49	>100	54.19 ± 2.55
8c	CH_3CH_2O	H	H	>100	64.47 ± 1.00	>100	37.03 ± 1.41
8d	H	CH_3O	H	>100	70.12 ± 1.71	>100	42.82 ± 1.07
8e	H	CH_3CH_2O	H	77.59 ± 1.77	55.61 ± 1.98	>100	37.41 ± 1.81
8f	H	$CH_3CH_2CH_2O$	H	57.59 ± 1.19	50.51 ± 2.12	>100	45.82 ± 3.33
8g	H	H	Br	64.81 ± 0.65	60.62 ± 1.32	80.78 ± 1.70	18.79 ± 2.70
8h	H		H	55.38 ± 0.24	30.76 ± 1.21	>100	18.47 ± 0.89
8i	H		H	17.13 ± 0.21	3.81 ± 0.13	67.14 ± 0.33	40.7 ± 0.79
8j	H		H	19.03 ± 0.11	3.13 ± 0.29	22.22 ± 1.25	24.97 ± 1.01
8k	H		H	8.48 ± 0.92	1.69 ± 0.34	16.6 ± 1.76	3.14 ± 0.63
8l	H		H	53.78 ± 1.71	38.26 ± 0.97	>100	71.85 ± 1.54
8m	H		H	52.08 ± 0.77	21.23 ± 0.683	>100	13.95 ± 0.94
8n	H		H	49.63 ± 1.36	13.23 ± 1.68	74.95 ± 1.90	15.57 ± 4.16
8o	H		H	80.63 ± 1.45	56.6 ± 0.73	68.15 ± 1.59	36.51 ± 1.84
8p	H		H	38.48 ± 1.98	12.26 ± 2.32	21.29 ± 1.02	17.95 ± 1.84
8q	H		H	23.14 ± 1.48	11 ± 0.69	48.86 ± 1.67	9.92 ± 1.43
8r	H	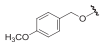	H	19.17 ± 0.88	4.51 ± 0.35	46.64 ± 1.41	12.51 ± 1.33
8s	H		H	13.3 ± 0.76	17.52 ± 0.14	42.98 ± 0.29	40.43 ± 1.86
8t	H		H	12.2 ± 0.28	6.55 ± 0.30	30.2 ± 1.04	25.42 ± 1.18
8u	H		H	10.41 ± 0.37	4.18 ± 0.87	22.72 ± 1.64	15.77 ± 0.75
Entinostat				4.02 ± 0.09	3.11 ± 0.04	6.36 ± 0.38	4.53 ± 0.13

[a] Mean ± S.D.; values are means of three independent experiments.

of HDAC1/HDAC than three other tested coumarins. Compounds **8f**, **8q** and **8r** also, exhibited significant inhibitory activity in the HDAC1 inhibition assay. These results demonstrated that coumarin ring is an effective surface recognition cap for HDAC1 inhibition.

2.2.4. *In vitro cytotoxicity of target compounds in normal cells*

To assess toxicity of target compounds in normal cells, Huvec cells were selected and treated with all of the compounds under the same conditions following a reported procedure [48]. As shown in Table 4, lots of compounds were nontoxic (IC_{50} > 100 μM). In vitro therapeutic index (IVTI) was calculated by comparing cytotoxicity activity (IC_{50}) of compounds against HCT116 cells, which showed best sensitivity to test compounds, with that of compounds against Huvec cell line. IVTI was found to be above 6. This data suggested selective toxicity for our compounds.

Table 2
Cytotoxic Activity and HDAC Inhibition (IC_{50} (μM)[a]) of compounds **8a-u** and Entinostat against Human colon cancer (HCT116) and Ovarian cancer (A2780) Cell Lines.

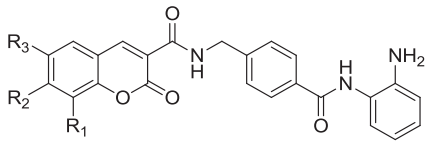

Compound	R_1	R2	R_3	cytotoxicityIC_{50}		HDAC inhibition		ClogP
				HCT116	A2780	HCT116	A2780	
8a	H	H	H	15.86 ± 0.72	61.87 ± 4.23	11.41 ± 0.87	54.92 ± 4.23	2.50
8b	CH_3O	H	H	9.04 ± 0.21	51.69 ± 1.35	5.17 ± 0.21	40.09 ± 1.35	2.43
8c	CH_3CH_2O	H	H	8.73 ± 0.35	45.67 ± 1.49	2.04 ± 0.49	32.86 ± 1.49	2.43
8d	H	CH_3O	H	8.16 ± 0.44	35.87 ± 1.31	3.08 ± 0.25	21.62 ± 1.31	2.43
8e	H	CH_3CH_2O	H	5.32 ± 0.25	29.95 ± 0.60	2.31 ± 0.44	17.04 ± 1.75	2.84
8f	H	$CH_3CH_2CH_2O$	H	3.34 ± 0.11	20.87 ± 2.38	1.09 ± 0.11	14.81 ± 2.38	3.29
8g	H	H	Br	7.70 ± 0.36	52.07 ± 2.40	6.64 ± 0.36	27.52 ± 2.21	3.23
8h	H		H	2.94 ± 0.18	19.51 ± 1.02	2.49 ± 0.18	12.82 ± 1.02	3.85
8i	H		H	1.65 ± 0.22	40.36 ± 1.49	1.40 ± 0.22	20.84 ± 1.49	4.20
8j	H		H	1.83 ± 0.51	19.13 ± 1.75	1.31 ± 0.33	10.10 ± 0.59	4.20
8k	H		H	0.27 ± 0.03	10.14 ± 1.75	0.25 ± 0.02	2.06 ± 0.10	4.20
8l	H		H	10.17 ± 1.15	42.90 ± 0.78	9.32 ± 0.50	17.33 ± 1.90	3.95
8m	H		H	5.30 ± 0.54	30.83 ± 1.12	3.73 ± 0.54	15.77 ± 1.12	3.95
8n	H		H	3.50 ± 0.56	15.37 ± 1.90	2.46 ± 0.47	9.72 ± 1.90	3.95
8o	H		H	6.55 ± 0.78	50.33 ± 1.45	4.76 ± 0.51	10.09 ± 1.45	4.46
8p	H		H	2.35 ± 0.32	31.22 ± 1.90	1.77 ± 0.27	6.04 ± 0.78	4.46
8q	H		H	0.53 ± 0.47	2.207 ± 0.91	0.42 ± 0.03	5.41 ± 1.75	4.58
8r	H	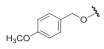	H	1.04 ± 0.27	27.53 ± 2.21	1.00 ± 0.12	6.52 ± 0.40	3.78
8s	H		H	7.66 ± 0.14	38.72 ± 1.50	6.14 ± 0.78	29.33 ± 1.50	5.06
8t	H		H	6.32 ± 0.57	27.57 ± 1.47	4.26 ± 0.32	23.86 ± 1.47	5.06
8u	H		H	1.76 ± 0.30	7.77 ± 0.31	0.80 ± 0.01	4.90 ± 0.31	5.06
Entinostat				2.03 ± 0.26	5.89 ± 0.21	1.96 ± 0.13	3.15 ± 0.21	4.52

[a] Mean ± S.D.; values are means of three independent experiments.

2.3. Molecular docking studies

In order to investigate the binding mode of the target compounds in the catalytic site of the HDAC1 (PDB ID: 4BKX), docking studies was carried out using Auto Dock 4.2. The best pose of each ligand in terms of free energy of binding was extracted from the 100 generated top poses the binding mode of compounds **8a**-**g** and the most potent compounds **8f**, **8q**, **8r, 8u** and Entinostat are shown in Fig. 4. Coumarins derivatives docked well to HDAC1 and bound similar to Entinostat.

The docking pose of **8a,** the simplest coumarin in the series, in complex with HDAC1 was shown in Figs. 5 and 6. HDAC1 is a zinc-dependent enzyme and its active site consisted of a long, narrow tunnel leading to a cavity that contains the catalytic Zn ion.

Table 3
HDAC1 inhibition activity (IC_{50} (μM)[a]) and isoform selectivity of **8f**, **8q**, **8r** and **8u**.

Compound	HDAC (HCT116)	HDAC (A2780)	HDAC1	HDAC1/HDAC (HCT116) Isoform selectivity	HDAC1/HDAC (A2780) Isoform selectivity
8f	1.09 ± 0.11	14.81 ± 2.38	0.87 ± 0.05	0.80	0.06
8q	0.42 ± 0.03	2.06 ± 0.21	0.50 ± 0.15	1.19	0.24
8r	0.80 ± 0.06	6.52 ± 0.40	0.71 ± 0.05	0.89	0.11
8u	1.00 ± 0.10	4.9 ± 0.31	0.47 ± 0.02	0.47	0.10
Entinostat	1.96 ± 0.13	3.15 ± 0.21	0.41 ± 0.06	0.21	0.13

[a] Mean ± S.D.; values are means of three independent experiments.

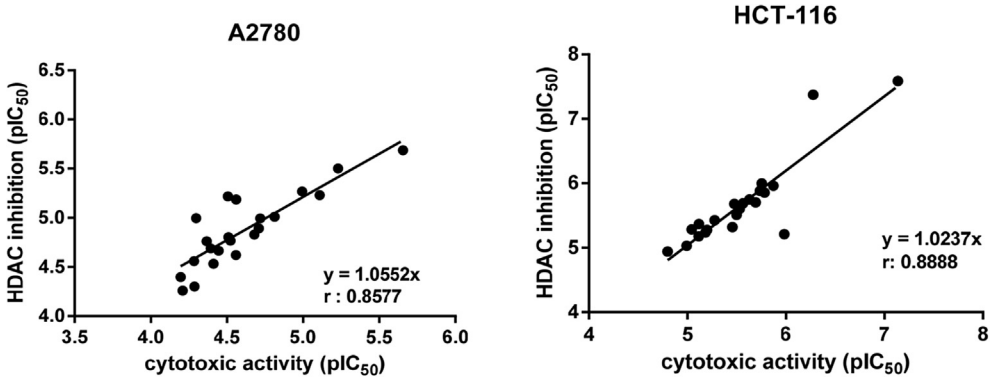

Fig. 3. Correlation between HDAC inhibition (HDAC inhibition assay, pIC50) and cytotoxic activity (MTT assay, pIC50) of all test compounds and Entinostat.

Zn ion was penta-coordinated with Asp176, His178 and Asp264 as well as the carbonyl and aniline of benzamide of compound **8a.** The protons of aniline formed hydrogen bonds with His140 and His 141 while NH of amide could also form a hydrogen binding interaction with Gly 149. The carbonyl oxygen of the benzamide group made hydrogen binding interaction with the phenolic hydroxyl group of Tyr303. Nevertheless, the aryl linker region of compound **8a** was located in the lipophilic tube including Leu271, Phe 205, Phe150, Met39 and Glu98. There was also π-π stacking interaction with benzene group of Phe150 which improved the binding affinity of compound **8a** to HDAC1.

Linear regression analysis of calculated binding affinities, K_i versus experimental cytotoxicity values, IC_{50} (Fig. 7.) showed that there was maximum correlation in case of HCT116 cells ($r = 0.88$; $r^2 = 0.78$) and minimum correlation in PC3 cells ($r = 0.58$; $r^2 = 0.35$).

2.4. Molecular dynamic simulation

Molecular dynamic simulation has been done to elucidate behavior of HDAC1 enzyme upon binding to inhibitor and stability and interaction of structure throughout simulation. The dynamic stability of secondary structure elements and conformational changes in ligand-bond protein were compared with apo-form of HDAC1 by root-mean-square derivations (RMSD) and root mean square fluctuation (RMSF) plots for 70 ns simulations.

RMSD is a measure of the stability of the structures. Fig. 8 showed that the RMSD of backbone (C_α, C, and N) of apo-form and ligand-bond protein **8a** reached stability after about 20ns of simulation. The average RMSD value of apo-form was 1.88 ± 0.133 A°, whereas the ligand-bond protein was also converged very close to apo-form with average RMSD value of 2.27 ± 0.15 A°. The average RMSD value of ligand **8a** was 0.04 ± 0.024 A° (Fig. S1) and ligand was stable during simulation. In RMSD of ligand-bond protein, the change was slightly larger than apo-form. It seemed that binding of ligand with protein increased the conformation flexibility of HDAC1 enzyme.

A root mean square fluctuation (RMSF) is an indicator of the macromolecular flexibility and indicates local changes in the protein structure [49]. The RMSF plots of apo-form and ligand-bond protein was illustrated in Fig. 9 and Fig. S2 in the Supplementary data. The protein structures of the two systems had similar RMSF distribution and same trends of dynamic features. The average RMSF of ligand-bond protein and apo-form were 0.73 ± 0.456 and 0.85 ± 0.533 A°, respectively. The relatively lower RMSF values of ligand-bond protein were found for residues located in the binding site (Asp176, His 178, Gly149, Asp264, His 140, and His 141and Tyr303). This could be explained by the relatively stronger binding of ligand with these residues that led to their less flexibility. The high fluctuating residues indicated that they were far from the active site or located in the loops (regions marked in bracket lines in Fig. 9) or terminals of protein.

To analyze in a more quantitative way, contribution of different residues at the active site (His140,His141, Gly149, Asp176, His178, Asp264 and Tyr303) in electrostatic, VdW and total interaction energy between ligand and HDAC1 was calculated (Fig. S3 in Supplementary data).

Radius of gyration (Rg) is a parameter that describes the equilibrium conformation of a total system and is an indicator of the protein structure compactness. As shown in Fig. 10, Rg values of the apo-form and ligand-bond protein **8a** were 20.53 ± 0.095 and 20.48 ± 0.085 A° (mean ± SD), respectively. The graphs showed that radius of gyration of apo-form was increased for the first 20 ns of simulation and then remained constant. It was observed that Rg of the ligand-bond protein was constant and larger than apo-form.

Hydrogen bonds play an essential role in stability ligand-protein complex. This stability of the hydrogen-bond network formed by the ligand in the protein active site analyzed in Fig. 11. The results showed that ligand formed three to four hydrogen bonds with protein. The benzamide group of ligand made three hydrogen bonds with His 140, His 141 and Gly 149 and also, the benzamide carbonyl of ligand could form strong bond with hydroxyl of Tyr 303.

These hydrogen bonds increased binding affinity of ligand with HDAC. The mean of intramolecular hydrogen bonds of the protein were 80 ± 7.19. These hydrogen bonds stabilized the secondary structure of HDAC1 (Fig. S4 in Supplementary data).

The percentage of protein secondary structures was investigated and it was found to be unchanged during simulation (Fig. S5 and S6 in Supplementary data).

Another simple way to measure the stability of system is potential energy. The ligand bond protein potential energy was found to be −33259.5 ± 13.35 kcal/mol indicating the stability of the system (Fig. S7 in Supplementary data).

The average distance between coordinated Zn^{2+} ion with active site residues (Asp176, His178 and Asp264) was in the range 2.02 ± 0.05 to 3.90 ± 0.19 A° (Fig. S8 in Supplementary data). In addition, the distance between carbonyl and amino groups of ligand with Zn^{2+} ion was in the range of 2.09 ± 0.07 to 2.21 ± 0.08 A°.These results improved the expected penta-coordination complex between HDAC1 residues and ligand with zinc ion at the enzyme active site. To discover the system condition during simulation, ligand bond protein structure was extracted from trajectories for each 5 ns (Fig. S9 in Supplementary data). These snapshots proved fixed orientation of ligand at the active site of the HDAC1 throughout simulation.

The 2D representation of the interaction between compound **8a** after 70ns simulation by LigPlot [50] has been depicted in Fig. 12.

2.5. ADME analysis

The ADME parameters of coumarin compounds and Entinostat as drug reference were measured using QikProp software (Table 5). All of the coumarins showed good partition coefficient (QplogPo/w) in permeable range of 2.90–5.62. The Caco-2 cell permeability (QPPCaco) was in the permissible range of 126.98–128.52. Also, the percentage human oral absorption for the compounds ranged from 70 to 86%. All of the parameters were within the acceptable range defined for human use and these compounds may exhibit significant pharmacokinetic and drug likeliness properties.

3. Conclusion

A new class of coumarin-based benzamides as HDAC inhibitors was designed, synthesized and evaluated for their in vitro antiproliferative activities by MTT assay against human cancer (HCT116, A2780, MCF7, PC3, HL60 and A549) and normal (Huvec) cell line as well as for pan HDAC and HDAC1 isoform inhibitory activities. Most of compounds exhibited significant cytotoxicity and potent HDAC inhibition activity. Four compounds (**8f**, **8q**, **8r** and **8u**) showed superior cytotoxicity activities (IC_{50} = 0.53–57.59 μM) on cancer cells and higher enzymatic pan HDAC (IC_{50} = 0.80–14.81 μM) and HDAC1 (IC_{50} = 0.47–0.87 μM) inhibitory activities and also, had no effect on Huvec viability (IC_{50} > 100 μM). Among them, **8u** displayed a higher potency for HDAC1 inhibition with IC_{50} value of 0.47 ± 0.02 μM comparable with Entinostat (IC_{50} = 0.41 ± 0.06 μM). Molecular docking studies of coumarin derivatives showed that they could bind tightly to the active site of HDAC1. Molecular dynamics simulation showed interaction mode of lead compound **8a** with HDAC1 including zinc ion coordination, strong hydrophobic interactions and formation of hydrogen bond with lead compound **8a**.These findings suggested that coumarin derivatives could be promising lead compounds for further development of anticancer agents through HDACs inhibition.

4. Experiment section

4.1. Chemistry

All reagents and solvents were purchased from Merck & Co., Inc. (Darmatadt, Germany) and Acros Organics (Thermofisher, Belgium) and used without further purification. Entinostat and vorinostat were purchased from EuroAsia Chemicals® (www.euroasiarnd.com). The progress of all reactions was monitored by thin-layer chromatography with 0.25 mm Silica gel plates (60 GF-254-Merck & Co (Darmatadt, Germany)) and visualized using UV light and iodine vapor. Melting points were measured with an electrothermal melting point apparatus (Stafford, UK) and were uncorrected. Infrared spectra were recorded on a Perkin Elmer Model 1420 spectrometer (KBr disks, Massachusetts, USA).^{1}H NMR and ^{13}CNMR spectra were determined at 300 MHz and 75 MHz, respectively (DMSO-d_6, TMS) on a Bruker FT-300 MHz instrument (Karlsruhe, Germany). The chemical shifts (δ) and coupling constants (J) are expressed in parts per million and Hertz, respectively. Spin multiples are given as s (singlet), d (doublet), t (triplet), q (quartet), s (sextet), m (multiplet). Mass spectra were obtained from a 6410 Agilent LC-MS triple quadrupole mass spectrometer (LC-MS, Santa Clara, USA) with an electrospray ionization (ESI) interface. Elemental analyses were performed on a Cos-Tec model EAS 4010 instrument (Cernusco, Italy) and the results are within ±0.4% of the theoretical values. Cell lines, including HCT116, A2780, MCF7, A549, HL60, PC3 and Huvec purchased from Pasteur Institute Cell Bank of IRAN (Tehran, IRAN).

4.2. General procedure for the synthesis of ethyl 2-oxo-2H-chromene-3-carboxylates (*3a-u*)

Diethyl malonate (2.11 mmol) and piperidine (2 mL) were added to a solution of the appropriate salicylaldehyde derivatives (**1a-e**) (10 mmol) in ethanol (20 mL) and the resulting mixture was refluxed for 14–15 h until the disappearance of the starting materials (monitored by TLC). After cooling, the crude product was filtrated, washed with cold ethanol and recrystallized from ethanol.

4.3. General procedure for the synthesis of ethyl 7-alkyl or aryl-2-oxo-2H-chromene-3-carboxylates (*3f-v*)

Potassium Carbonate (6 mmol) was added to ethyl 7-hydroxy-2-oxo-2H-chromene-3-carboxylate (**3e**, 5 mmol) in DMF (20 mL) and the mixture was stirred at rt for several minutes, then appropriate alkyl halide or benzyl halide derivatives (14 mmol) were added dropwise to the mixture and stirred for 10–12 h. Upon completion, water is added to the mixture and the produced precipitate was filtrated, washed with water and used in the next step without further purification.

4.4. General procedure for the synthesis of 2-oxo-2H-chromene-3-carboxylic acids (*4a-u*)

Esters (3a-v) were dissolved in aqueous sodium hydroxide (2 N, 20 mL) and were stirred at rt for 5–7 h. After cooling, solution was acidified with hydrochloric acid (2 N) until a white precipitate formed. The white solid was filtrated, washed with water and dried to yield acids (**4a-u**).

4.5. General procedure for the synthesis of 4-((2-oxo-2H-chromene-3-carboxamido) methyl) benzoic acid derivatives (*6a-u*)

the corresponding 2-oxo-2H-chromene-3-carboxylic acids (**3a-v**, 5 mmol) was added to a suspension of 1, 1′-carbonyldimidazole

Table 4
The in vitro cell proliferation activities (IC_{50} (μM)[a]) of compounds **8a-u** and Entinostat against human normal cell line.

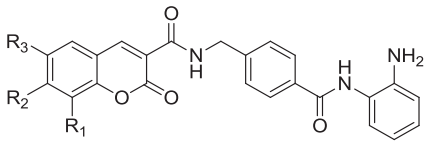

Compound	Huvec	In vitro therapeutic index (Huvec IC_{50}/HCT116 IC_{50})
8a	>100	>6.30
8b	>100	>11.06
8c	>100	>11.45
8d	>100	>12.25
8e	>100	>18.80
8f	>100	>29.94
8g	76.287 ± 2.33	9.90
8h	50.51 ± 1.00	17.18
8i	49.553 ± 4.77	30.03
8j	20.833 ± 3.91	11.38
8k	40.8 ± 5.73	>50
8l	61.833 ± 2.43	6.07
8m	57.68 ± 1.02	10.88
8n	75.58 ± 3.01	21.59
8o	>100	>15.26
8p	>100	>42.55
8q	>100	>50
8r	>100	>50
8s	>100	>13.05
8t	>100	>15.82
8u	>100	>56.8
Entinostat	>100	>49.26

[a] Mean ± S.D.; values are means of three independent experiments.

(CDI, 25 mmol) in dry tetrahydrofuran (THF, 10 mL) and the mixture was stirred for 2 h at rt. Then 4-(aminomethyl) benzoic acid (**5**, 25 mmol) and trifluoroacetic acid (TFA, 1.2 mL) were added and stirred for additional 10 h at rt. The mixture was evaporated to remove THF and extracted with EtOAc, dried over anhydrous Na_2SO_4 and concentrated under reduced pressure. Further purification was done with preparative thin layer chromatography for some compounds (**6p** and **6q**). Due to very low solubility of compounds **6g**, **6i** and **6m**, we could not report 13C NMR data for these compounds.

*4.5.1. 4-((2-oxo-2H-chromene-3-carboxamido) methyl) benzoic acid (**6a**)*

White solid; yield:78%; mp: 261–263 °C; R_f = 0.56 (petroleum ether: ethyl acetate = 3:1); IR (KBr): ν_{max} (cm^{-1}) 3312 (NH), 1709 1602 (CO); ^{1}H NMR (300 MHz, DMSO-d_6) δ 4.63 (d, 2H, J = 6.0 Hz,CH_2), 7.44–7.54 (m, 4H, Ar-H), 7.77 (t, 1H, J = 6.0 Hz, Ar-H), 7.92 (d, 2H, J = 9.0 Hz, Ar-H), 7.99 (d, 1H, J = 9.0 Hz, Ar-H), 8.90 (s, 1H, CH), 9.23 (t, 1H, J = 6.0 Hz, NH); ^{13}C NMR (75 MHz, DMSO-d_6) δ 43.04, 116.62, 118.94, 119.57, 125.62, 127.78, 129.88, 130.06, 130.75, 134.61, 144.56, 148.08, 154.40, 160.73, 161.96, 167.60; Anal. calcd. for $C_{18}H_{13}NO_5$: C, 66.87; H, 4.05; N, 4.33; found: C 66.80, H 4.09, N 4.24.

*4.5.2. 4-((8-methoxy-2-oxo-2H-chromene-3-carboxamido) methyl) benzoic acid (**6b**)*

White solid; yield: 73%; mp: 238–240 °C; R_f = 0.49 (petroleum ether: ethyl acetate = 3:1); IR (KBr): ν_{max} (cm^{-1}) 3347 (NH), 1712 &1606 (CO); ^{1}H NMR (300 MHz, DMSO-d_6) δ 3.95 (s, 1H, OCH_3), 4.62 (d, 2H, J = 6.0 Hz, CH_2), 7.35–7.54 (m, 5H, Ar-H),7.91 (d, 1H, J = 8.1 Hz, Ar-H), 8.85 (s, 1H, CH), 9.24 (t, 1H, J = 5.7 Hz, NH); ^{13}C NMR (75 MHz, DMSO-d_6) δ 43.05, 56.65, 116.53, 119.46, 119.57, 121.62, 125.54, 127.81, 129.36, 137.81, 143.69, 144.56, 146.73, 148.30, 160.44, 161.83, 167.60; Anal. calcd. for $C_{19}H_{15}NO_6$: C, 64.59; H, 4.28; N, 3.96; found: C 64.66, H 4.20, N 4.05.

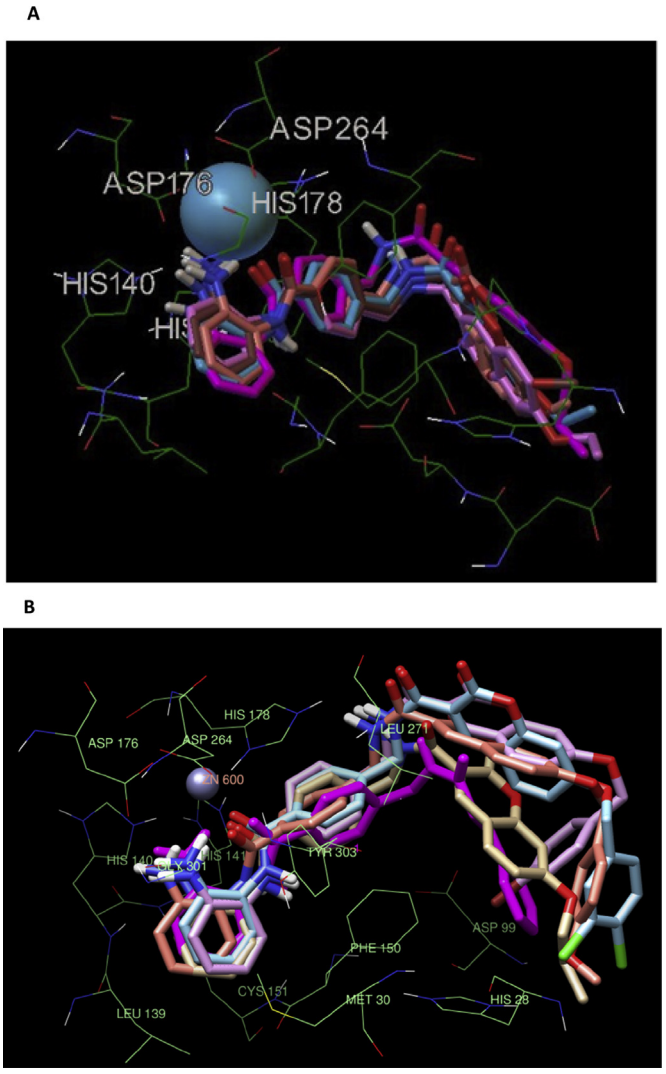

Fig. 4. The best pose of the compounds obtained from docking study in the active site of HDAC1. A; (compounds **8a**-**8g**). B; (compounds **8f**, **8q**, **8r, 8u** and Entinostat (in pink)). The important residues of binding site (Asp264, His178, and Asp176) and zinc ion were shown. (For interpretation of the references to colour in this figure legend, the reader is referred to the web version of this article.)

*4.5.3. 4-((8-ethoxy-2-oxo-2H-chromene-3-carboxamido) methyl) benzoic acid (**6c**)*

Pale yellow solid; yield: 79%; mp: 246–248 °C; R_f = 0.43 (petroleum ether: ethyl acetate = 3:1); IR (KBr): ν_{max} (cm^{-1}) 3335 (NH), 1707 and 1653 (CO); ^{1}H NMR (300 MHz, DMSO-d_6) δ 1.42 (t, 3H, J = 6.9Hz, CH_3), 4.20 (q, 2H, J = 6.9Hz,OCH_2), 4.62 (d, 2H, J = 6.0Hz, CH_2), 7.34 (d, 1H, J = 7.5Hz, Ar-H), 7.42–7.48 (m, 3H, Ar-H), 7.52 (dd, 1H, J_1 = 7.5Hz, J_2 = 1.2Hz, Ar-H), 7.92 (d, 2H, J = 8.1Hz, Ar-H), 8.86 (s, 1H, CH), 9.23 (t, 1H, J = 6.0Hz, NH); ^{13}C NMR (75 MHz, DMSO-d_6) δ 15.04, 43.03, 65.02, 117.43, 119.56, 119.59, 121.62, 125.56, 127.82, 129.89, 137.82, 143.79, 144.63, 145.98, 148.37, 160.53, 161.96, 167.66; Anal. calcd. for $C_{20}H_{17}NO_6$: C, 65.39; H, 4.66; N, 3.81; found: C 65.30, H 4.73, N 3.75.

*4.5.4. 4-((7-methoxy-2-oxo-2H-chromene-3-carboxamido) methyl) benzoic acid (**6d**)*

Light brown; yield: 89%; mp: 242–244 °C; R_f = 0.46 (petroleum

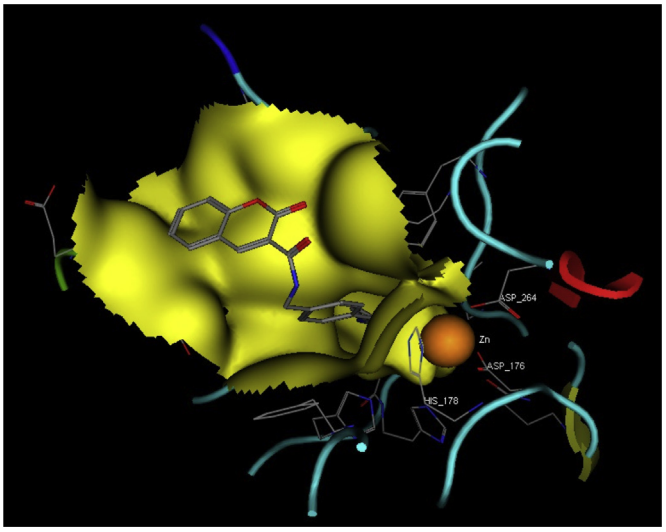

Fig. 5. 3D representation of docked ligand **8a** into the tunnel-like binding site of HDAC1.

148.47, 156.64, 161.24, 162.20, 164.90, 167.65; Anal. calcd. for $C_{19}H_{15}NO_6$: C, 64.59; H, 4.28; N, 3.96; found: C 64.48, H 4.34, N 3.89.

*4.5.5. 4-((7-ethoxy-2-oxo-2H-chromene-3-carboxamido) methyl) benzoic acid (**6e**)*

Pale yellow solid; yield: 85%; mp: 245–247 °C; R_f = 0.59 (petroleum ether: ethyl acetate = 3:1)

IR (KBr): ν_{max} (cm^{-1}) 3339 (NH), 1718, 1654 and 1613 (CO); ^1H NMR (300 MHz, DMSO-d_6) δ 1.38 (t, 3H, J = 6.6Hz, CH_3), 4.18 (q, 2H, J = 6.9Hz, OCH_2), 4.67 (d, 2H, J = 6.6Hz, CH_2), 7.05 (m, 2H, Ar-H), 7.50 (d, 2H, J = 7.8Hz, Ar-H), 7.92 (d, 2H, J = 6.9Hz, Ar-H), 8.10 (d, 1H, J = 7.8Hz, Ar-H), 8.86 (s, 1H, CH), 9.20 (t, 1H, J = 7.8Hz, NH), 12.90 (brs, 1H, OH); ^{13}C NMR (75 MHz, DMSO-d_6) δ 14.82, 42.84, 64.89, 101.49, 112.49, 114.38, 115.14, 127.79, 129.70, 129.90, 131.03, 144.86, 148.54, 156.71, 161.28, 162.17, 164.22, 167.54; Anal. calcd. for $C_{20}H_{17}NO_6$: C, 65.39; H, 4.66; N, 3.81; found: C 65.29, H 4.75, N 3.74.

*4.5.6. 4-((2-oxo-7-propoxy-2H-chromene-3-carboxamido) methyl) benzoic acid (**6f**)*

Yellow solid; Yield: 82%; mp: 259–261 °C; R_f = 0.55 (petroleum ether: ethyl acetate = 3:1)

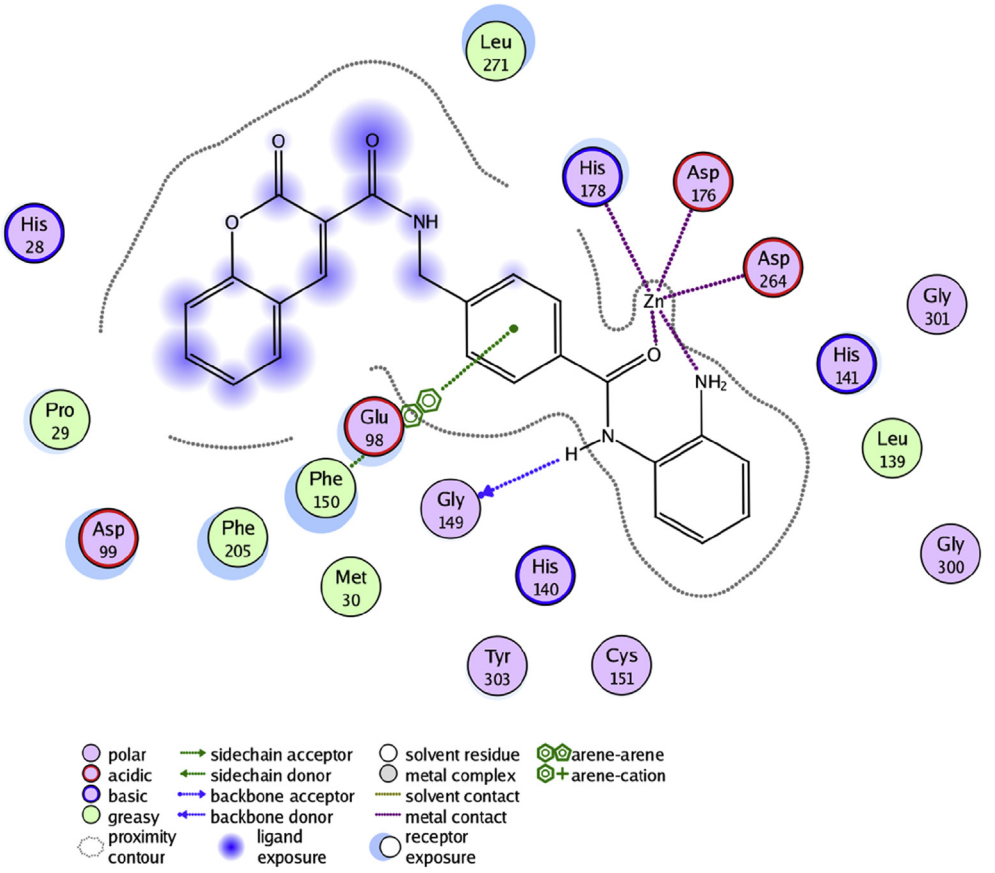

Fig. 6. The 2D representation of the interaction between compound **8a** in the crystal structure of HDAC1.

ether: ethyl acetate = 3:1); IR (KBr): ν_{max} (cm^{-1}) 3346 (NH), 1701, 1659 &1614 (CO); ^1H NMR (300 MHz, DMSO-d_6) δ 3.89 (s, 3H, OCH_3), 4.62 (d, 2H, J = 6.0Hz, CH_2), 7.02 (dd, 1H, J_1 = 8.7Hz, J_2 = 2.4Hz, Ar-H), 7.09 (d, 1H, J = 2.1Hz, Ar_H), 7.45 (d, 2H, J = 8.1Hz, Ar-H), 7.90 (m, 3H, Ar-H), 8.83 (s, 1H, CH), 9.17 (t, 1H, J = 6.0Hz, NH), 12.91 (brs, 1H, OH); ^{13}C NMR (75 MHz, DMSO-d_6) δ 42.98, 56.67, 100.69, 112.54, 114.05, 115.16, 127.77, 129.84, 129.90, 131.99, 144.77,

IR (KBr): ν_{max} (cm^{-1}) 3333 (NH), 1701, 1659 and 1618 (CO); ^1H NMR (300 MHz, DMSO-d_6) δ 1.00 (t, 3H, J = 7.2Hz, CH_3), 1.77 (se, 2H, J = 6.9Hz, CH_2), 4.10 (t, 2H, J = 6.6Hz, OCH_2), 4.62 (d, 1H, J = 6.0Hz, CH_2), 7.04 (dd, 1H, J_1 = 8.7Hz, J_2 = 2.4Hz, Ar-H), 7.11 (d, 1H, J = 2.1Hz, Ar-H), 7.45 (d, 2H, J = 8.4Hz, Ar-H), 7.89–7.93 (m, 3H, Ar-H), 8.86 (s, 1H, CH), 9.19 (t, 1H, J = 6.0Hz, NH); ^{13}C NMR (75 MHz, DMSO-d_6) δ 10.75, 22.23, 42.95, 70.55, 110.13, 112.49, 114.40, 115.12, 127.78,

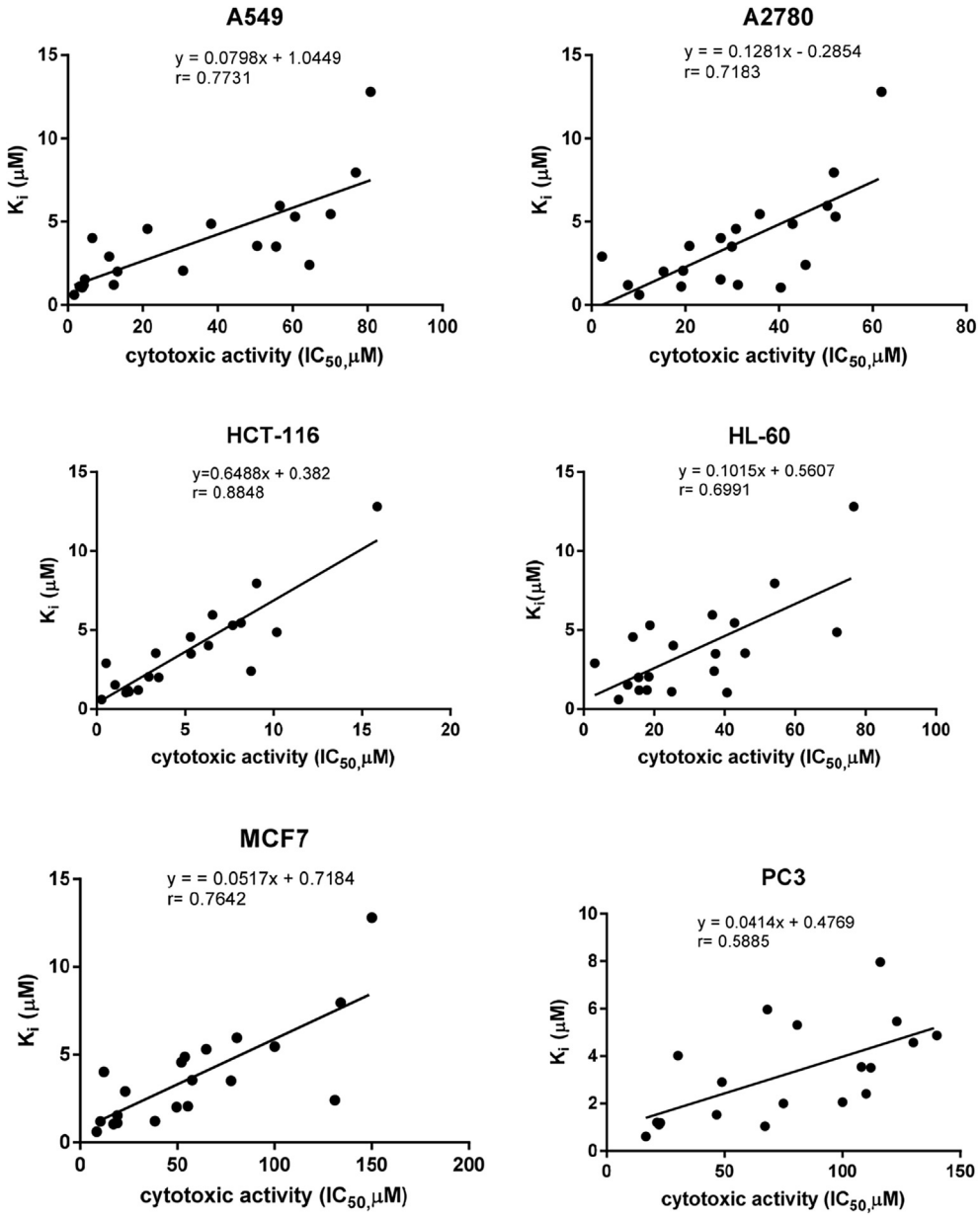

Fig. 7. Linear regression analysis of predicted HDAC1 binding affinities (K_i) versus experimental cytotoxic effects (IC_{50}).

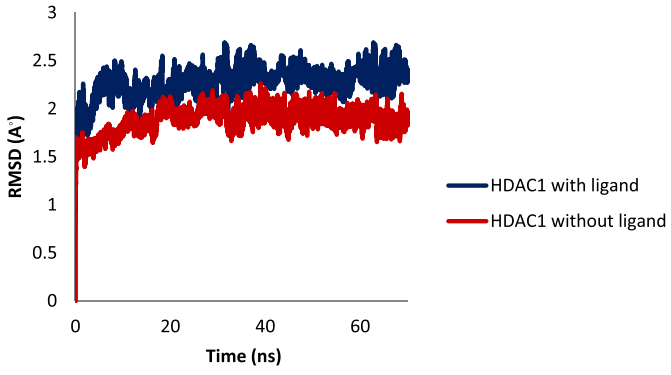

Fig. 8. RMSD between HDAC1 with ligand and without ligand.

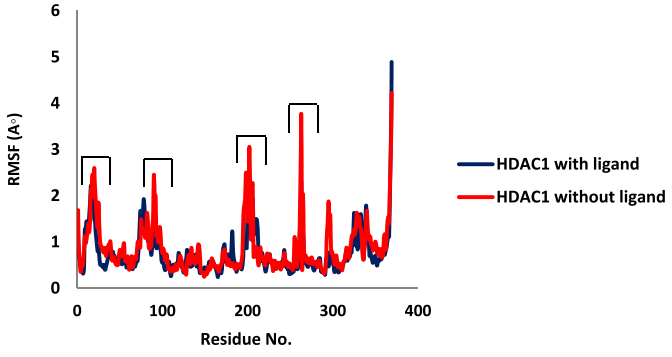

Fig. 9. Per residue RMSF of HDAC1 with ligand and without ligand during 70 ns simulation. Residues with RMSF greater than 2A° were marked in braket lines.

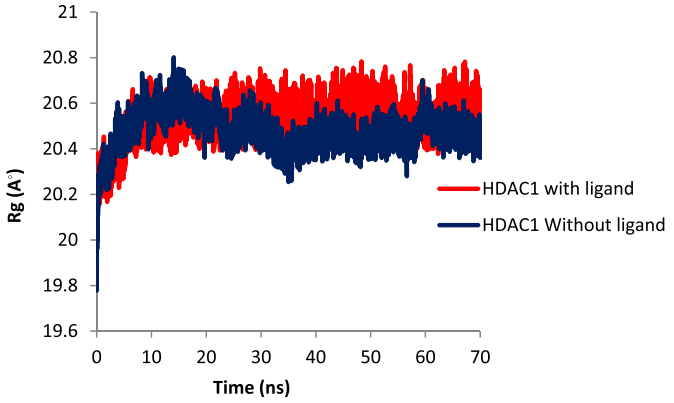

Fig. 10. Rg of HDAC1 with ligand and without ligand.

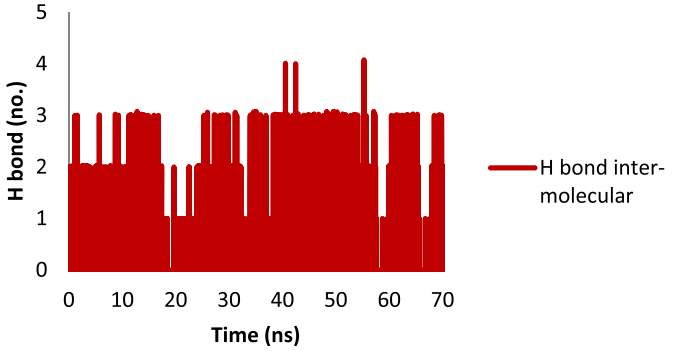

Fig. 11. Number of hydrogen bonds between HDAC1 and ligand in time scale.

129.72, 129.90, 132.08, 144.84, 148.54, 156.71, 161.26, 162.18,164.38, 167.56; Anal. calcd. for $C_{21}H_{19}NO_6$: C, 66.13; H, 5.02; N, 3.67; found: C 65.20, H 4.93, N 3.73.

*4.5.7. 4-((6-bromo-2-oxo-2H-chromene-3-carboxamido) methyl) benzoic acid (**6g**)*

White solid; yield: 86%; mp: 295–297 °C; $R_f = 0.46$ (petroleum ether: ethyl acetate = 3:1); IR (KBr): ν_{max} (cm^{-1}) 3349 (NH), 1713, 1653 and 1611 (CO); ^1H NMR (300 MHz, DMSO-d_6) δ 4.62 (d, 2H, CH_2), 7.44–7.51 (m, 3H, Ar-H), 7.88–7.93 (m, 3H, Ar-H), 8.26 (d, 1H, J = 2.1Hz, Ar-H), 8.84 (s, 1H, CH), 9.21 (t, 1H, J = 6.0Hz, NH); Anal. calcd. for $C_{18}H_{12}BrNO_5$: C, 53.75; H, 3.01; N, 3.48; found: C 53.68, H 3.10, N 3.37.

*4.5.8. 4-((2-oxo-7-phenoxy-2H-chromene-3-carboxamido) methyl) benzoic acid (**6h**)*

Yellow solid; yield:85%; mp: 245–247 °C; $R_f = 0.34$ (petroleum ether: ethyl acetate = 3:1); IR (KBr): ν_{max} (cm^{-1}) 3340 (NH), 1705, 1658 and 1613 (CO); ^1H NMR (300 MHz, DMSO-d_6) δ 4.61 (d, 2H, J = 6.0Hz, CH_2), 5.28 (s, 2H, CH_2), 7.12 (dd, 1H, J_1 = 8.7Hz, J_2 = 2.1 Hz, Ar-H), 7.21 (d, 1H, J = 2.1Hz, Ar-H), 7.35 (m, 7H, Ar-H), 7.91 (m, 3H, Ar-H), 8.85(s. 1H, CH_1), 9.18 (t, 1H, NH), 12.89 (s, 1H, OH); ^{13}C NMR (75 MHz, DMSO-d_6) δ 42.96, 70.68, 101.66, 112.77, 114.65, 115.46, 127.07, 127.79, 128.51, 128.72, 129.05, 129.90, 132.12, 136.44, 144.83, 148.45, 156.58, 161.22, 162.25, 163.91, 167.59; Anal. calcd. for $C_{25}H_{19}NO_6$: C, 69.92; H, 4.46; N, 3.26; found: C 69.90, H 4.39, N 3.32.

*4.5.9. 4-((2-oxo-7-(o-tolyloxy)-2H-chromene-3-carboxamido) methyl) benzoic (**6i**)*

Pink solid; yield: 83%; mp: 229–231 °C; $R_f = 0.45$ (petroleum ether: ethyl acetate = 3:1); IR (KBr): ν_{max} (cm^{-1}) 3342 (NH), 1705, 1657 &1610 (CO); ^1H NMR (300 MHz, DMSO-d_6) δ 2.33 (s, 3H, CH_3), 4.61 (d, 2H, J = 5.7Hz, CH_2), 5.24 (s, 2H, OCH_2), 7.10 (dd, 1H, J_1 = 8.7Hz, J_2 = 2.1Hz, CH_2), 7.19–7.25 (m, 4H, Ar-H), 7.43–7.47 (m, 3H, Ar-H) 7.89–7.94 (m, 3H, Ar-H), 8.85 (s, 1H, CH), 9.18 (t, 1H, J = 6.0Hz, NH), 12.89 (s, 1H, OH); Anal. calcd. for $C_{26}H_{21}NO_6$: C, 70.42; H, 4.77; N, 3.16; found: C 70.50, H 4.73, N 3.25.

*4.5.10. 4-((2-oxo-7-(m-tolyloxy)-2H-chromene-3-carboxamido) methyl)benzoic acid (**6j**)*

Pale yellow solid; Yield:85%; mp: 228–230 °C; $R_f = 0.30$ (petroleum ether: ethyl acetate = 3:1); IR (KBr): ν_{max} (cm^{-1}) 3331 (NH), 1703, 1655 & 1618 (CO); ^1H NMR (300 MHz, DMSO-d_6) δ 2.24 (s, 3H, CH_3), 4.62 (d, 2H, J = 6.0Hz,CH_2), 5.23 (s, 2H, OCH_2), 7.07–7.34 (m,6H, Ar-H), 7.44 (d, 2H, J = 8.1Hz, Ar-H), 7.90–7.94 (m, 3H, Ar-H), 8.86 (s, 1H, CH), 9.18 (t, 1H, J = 6.0Hz, NH), 12.93 (s, 1H, OH); ^{13}C NMR (400 MHz, DMSO-d_6) δ 21.45, 42.97, 70.73, 101.61, 112.75, 114.63, 115.42, 125.60, 127.78, 128.94, 129.05, 129.33, 129.82,132.10, 136.34,138.24, 144.81, 148.46, 156.58, 161.23, 162.23, 163.94, 167.63; Anal. calcd. for $C_{26}H_{21}NO_6$: C, 70.42; H, 4.77; N, 3.16; found: C 70.52, H 4.70, N 3.23.

*4.5.11. 4-((2-oxo-7-(p-tolyloxy)-2H-chromene-3-carboxamido) methyl)benzoic acid (**6k**)*

Pale yellow solid; Yield:89%; mp: 264–266 °C; $R_f = 0.35$ (petroleum ether: ethyl acetate = 3:1)

IR (KBr): ν_{max} (cm^{-1}) 3321 (NH), 1700, 1651 & 1611(CO); ^1H NMR (300 MHz, DMSO-d_6) δ 2.36 (s, 3H, CH_3), 4.65 (d, 2H, J = 6.0Hz, CH_2),5.27 (s, 1H, OCH_2) 7.14 (dd, 1H, J_1 = 8.7Hz, J_2 = 2.4Hz, Ar-H), 7.24–7.28 (m, 3H, Ar-H), 7.41 (d, 2H, J = 8.1Hz, Ar-H), 7.48 (d, 2H, J = 8.1Hz, Ar-H), 7.94–7.97 (m, 3H, Ar-H), 8.90 (s, 1H, CH), 9.22 (t, 1H, J = 6.0Hz, NH), 12.97 (s, 1H, OH); ^{13}C NMR (75 MHz, DMSO-d_6) δ 21.26, 42.97, 70.60, 101.64, 112.71, 114.66, 115.39, 127.78, 128.61, 129.36, 129.57, 129.89, 132.08, 133.39,138.02, 144.80, 148.46, 156.58, 161.23, 162.23, 163.94, 167.64; Anal. calcd. for $C_{26}H_{21}NO_6$: C, 70.42; H, 4.77; N, 3.16; found: C 70.35, H 4.83, N 3.18.

*4.5.12. 4-((7-(2-fluorophenoxy)-2-oxo-2H-chromene-3-carboxamido) methyl) benzoic acid (**6l**)*

Yellow solid; yield: 92%; mp: 238–240 °C; $R_f = 0.38$ (petroleum ether: ethyl acetate = 3:1); IR (KBr): ν_{max} (cm^{-1}) 3340 (NH), 1713, 1695 and 1616 (CO); ^1H NMR (300 MHz, DMSO-d_6) δ 4.61 (d, 2H, J = 6.0 Hz,CH_2), 5.31 (s, 2H, OCH_2), 7.13 (dd, 1H, J_1 = 8.7Hz, J_2 = 2.4Hz, Ar-H), 7.25–7.33 (m, 3H, Ar-H), 7.45 (m, 3H, Ar-H), 7.62 (t, 1H, J = 7.2Hz, Ar-H), 7.90–7.96 (m, 3H, Ar-H), 8.86 (s, 1H, CH), 9.19 (t, 1H, J = 6.0Hz, NH), 12.93 (1H, OH); ^{13}C NMR (75 MHz, DMSO-d_6) δ 42.98, 65.07, 101.55, 112.90, 114.44, 115.55, 115.86, 123.33, 125.14, 127.77, 129.90, 131.45, 131.56, 131.61, 132.14, 144.77, 148.41, 156.55, 159.39, 161.21, 162.21, 163.67, 167.66; Anal. calcd. for $C_{25}H_{18}FNO_6$: C, 67.11; H, 4.06; N, 3.13; found: C 67.20, H 4.12, N 3.04.

*4.5.13. 4-((7-(3-fluorophenoxy)-2-oxo-2H-chromene-3-carboxamido) methyl) benzoic acid (**6m**)*

Pale yellow solid; yield: 80%; mp: 259–261 °C; $R_f = 0.39$ (petroleum ether: ethyl acetate = 3:1); IR (KBr): ν_{max} (cm^{-1}) 3338 (NH), 1711, 1657 and 1614 (CO); ^1H NMR (300 MHz, DMSO-d_6) δ 4.61 (d, 2H, J = 6.0 Hz,CH_2), 5.30 (s, 2H, OCH_2), 7.13–7.23 (m, 3H, Ar-H), 7.33 (d, 2H, J = 7.2Hz, Ar-H), 7.44–7.52 (m, 3H, Ar-H), 7.90–7.96 (m, 3H, Ar-H), 8.86 (s, 1H, CH), 9.18 (t, 1H, J = 6.0Hz, NH), 12.94 (brs, 1H, OH); Anal. calcd. for $C_{25}H_{18}FNO_6$: C, 67.11; H, 4.06; N, 3.13; found: C 67.22, H 4.00, N 3.20.

*4.5.14. 4-((7-(4-fluorophenoxy)-2-oxo-2H-chromene-3-carboxamido)methyl)benzoic acid (**6n**)*

Yellow solid; yield: 92%; mp: 266–268 °C; $R_f = 0.43$ (petroleum ether: ethyl acetate = 3:1); IR (KBr): vmax (cm^{-1}) 3338 (NH), 1704,

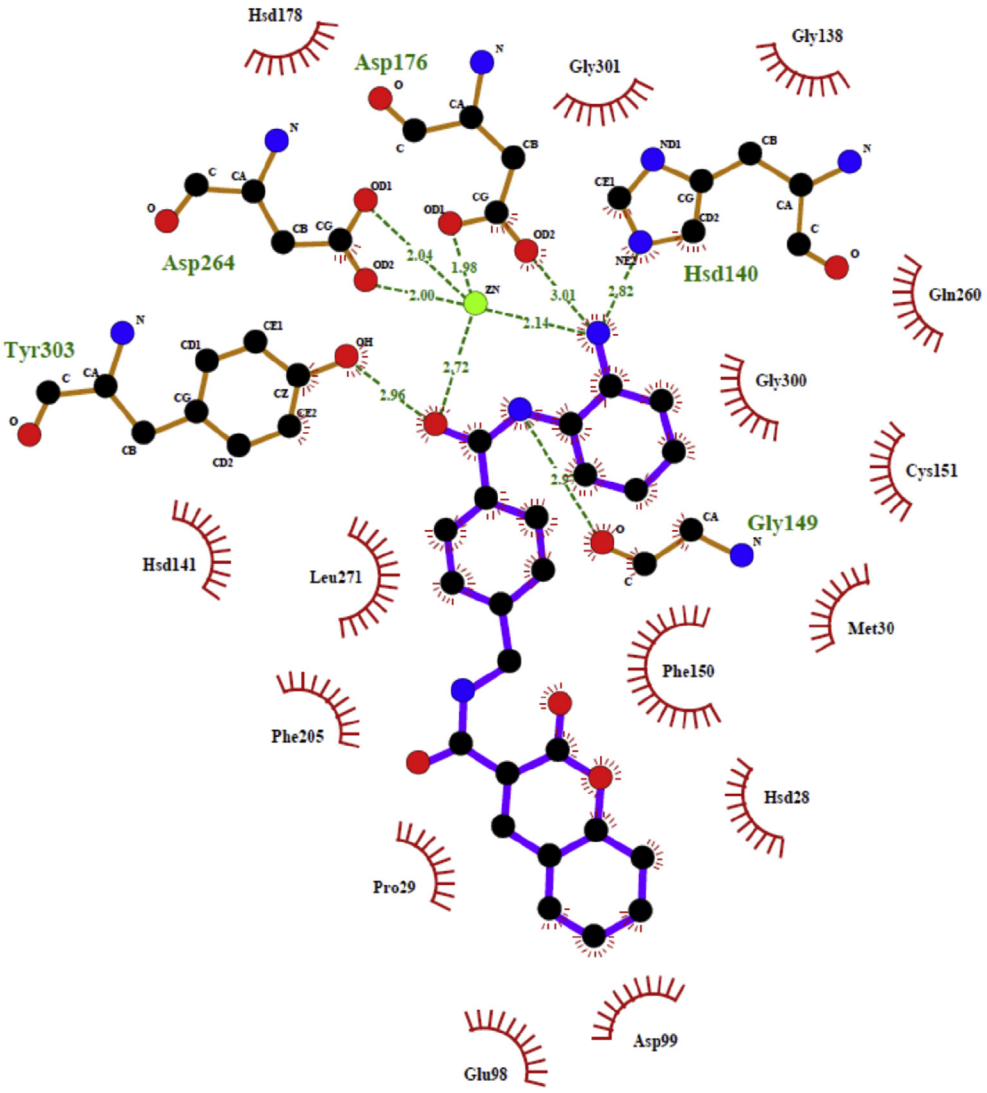

Fig. 12. A diagrammatic represention of interactions between ligand **8a** and HDAC1 at the active site after 70ns molecular dynamic simulation. The green dotted lines represent hydrogen bond interaction and red arcs with radiating spokes represents the amino acids showing hydrophobic interaction with protein. Carbon, nitrogen and oxygen atoms have been shown in black, blue and red, respectively. The violet lines represent the ligand bond. (For interpretation of the references to colour in this figure legend, the reader is referred to the web version of this article.)

1653 and 1617 (CO); ^{1}H NMR (300 MHz, DMSO-d_6) δ 4.61 (d, 2H, J = 6.0 Hz,CH_2), 5.25 (s, 2H, OCH_2), 7.12 (dd, 1H, $J1$ = 8.5Hz, J_2 = 2.1Hz, Ar-H), 7.21–7.29 (m, 3H, Ar-H), 7.44 (d, 2H, J = 8.1Hz, Ar-H), 7.53–7.60 (m, 2H, Ar-H), 7.90–7.94 (m, 3H, Ar-H), 8.86 (s, 1H, CH), 9.18 (t, 1H, J = 6.0Hz, NH); ^{13}C NMR (75 MHz, DMSO-d_6) δ 42.97, 69.94, 101.64, 112.79, 114.61, 115.48, 115.74, 116.02, 127.77, 129.89, 130.81, 131.79, 132.11, 132.66, 144.73, 148.43, 156.56, 161.21, 162.15, 163.78, 167.66; Anal. calcd. for $C_{25}H_{18}FNO_6$: C, 67.11; H, 4.06; N, 3.13; found: C 67.04, H 3.97, N 3.23.

*4.5.15. 4-((7-(2-chlorophenoxy)-2-oxo-2H-chromene-3-carboxamido) methyl) benzoic acid (**6o**)*

Yellow solid; yield: 75%; m: 262–264 °C; R_f = 0.33 (petroleum ether: ethyl acetate = 3:1); IR (KBr): ν_{max} (cm^{-1}) 3342 (NH), 1705, 1659 and 1616 (CO); ^{1}H NMR (300 MHz, DMSO-d_6) δ 4.62 (d, 2H, J = 6.0Hz, CH_2), 5.37 (s, 2H, OCH_2), 7.20 (dd, 1H, J_1 = 8.7Hz, J_2 = 2.4Hz, Ar-H), 7.33 (d, 1H, J = 2.4Hz, Ar-H), 7.44–7.53 (m, 4H, Ar-H), 7.61 (m, 1H, Ar-H), 7.71 (m, 1H, Ar-H), 7.95-7-8.02 (m, 3H, Ar-H), 8.92 (s, 1H, CH), 9.24 (t, 1H, J = 6.0Hz, NH), 12.95 (s, 1H, OH); ^{13}C NMR (75 MHz, DMSO-d_6) δ 42.98, 68.42, 101.63, 112.97, 114.44, 115.63, 127.80, 127.98, 129.74, 129.90, 130.03, 130.90, 131.30, 132.19, 133.59, 133.73, 144.84, 148.42, 156.57, 161.20, 162.14, 163.70, 167.55; Anal. calcd. for $C_{25}H_{18}ClNO_6$: C, 64.73; H, 3.91; N, 3.02; found: C 64.67, H 4.01, N 3.09.

*4.5.16. 4-((7-(4-chlorophenoxy)-2-oxo-2H-chromene-3-carboxamido) methyl) benzoic acid (**6p**)*

Yellow solid; yield: 80%; mp: 270–272 °C; R_f = 0.36 (petroleum ether: ethyl acetate = 3:1)

IR (KBr): ν_{max} (cm^{-1}) 3340 (NH), 1703, 1656 and 1610 (CO); ^{1}H NMR (300 MHz, DMSO-d_6) δ 4.61 (d, 2H, J = 6.0Hz, CH_2), 5.28 (s, 2H, OCH_2), 7.12 (dd, 1H, J_1 = 8.7Hz, J_2 = 2.4Hz, Ar-H), 7.22 (d, 1H, J = 2.4Hz, Ar-H), 7.44–7.55 (m, 6H, Ar), 7.90–7.95 (m, 3H, Ar-H), 8.86 (s, 1H, CH), 9.18 (t, 1H, J = 6.0Hz, NH), 12.95 (s, 1H, OH); ^{13}C NMR (75 MHz, DMSO-d_6) δ 42.97, 69.78, 101.70, 112.86, 114.53, 115.57, 127.78, 129.05, 129.83, 129.89, 130.33, 132.13, 133.30, 135.51, 144.79, 148.41, 156.55, 161.19, 162.22, 163.68, 167.63; Anal. calcd. for $C_{25}H_{18}ClNO_6$: C, 64.73; H, 3.91; N, 3.02; found: C 64.80, H 3.83, N 3.10.

Table 5
ADME and pharmacological parameter prediction for the coumarin compounds using QikProp.

Compound	QPlogPo/w[a]	QPPCaco[b]	QPlogBB[c]	QPlogHERG[d]	Percent Human Oral Absorption[e]	QPlogKp[f]	#metab[g]
8a	2.905	126.985	−2.002	−7.5	81.608	−2.88	5
8b	2.998	123.45	−2.136	−7.405	81.936	−3	6
8c	3.438	127.065	−2.296	−7.704	84.731	−2.881	6
8d	3.459	127.274	−1.865	−7.42	84.869	−3.046	5
8e	3.003	127.281	−2.095	−7.317	82.202	−2.987	6
8f	3.423	127.86	−2.235	−7.518	84.692	−2.903	6
8g	3.809	127.632	−2.396	−7.797	86.939	−2.791	6
8h	4.741	127.213	−2.467	−8.909	79.415	−2.097	7
8i	4.928	127.019	−2.424	−8.577	80.499	−2.265	8
8j	5.035	127.492	−2.501	−8.702	68.194	−2.309	8
8k	5.047	127.083	−2.522	−8.764	68.241	−2.299	8
8l	4.875	127.592	−2.384	−8.757	80.224	−2.19	7
8m	4.953	127.668	−2.362	−8.742	80.681	−2.234	7
8n	4.94	128.263	−2.341	−8.679	80.642	−2.245	7
8o	5.069	124.962	−2.337	−8.696	68.235	−2.245	7
8p	5.225	128.14	−2.325	−8.764	69.343	−2.263	7
8q	5.29	127.97	−2.317	−8.765	69.716	−2.271	7
8r	4.831	127.832	−2.553	−8.688	79.976	−2.209	8
8s	5.489	124.634	−2.222	−8.577	70.676	−2.38	7
8t	5.553	124.588	−2.202	−8.557	71.047	−2.418	7
8u	5.627	128.523	−2.182	−8.563	71.725	−2.414	7
Entinostat	2.388	144.236	−1.957	−7.014	79.569	−2.944	8

[a] Predicted octanol/water partition coefficient (acceptable range: −2.0–6.5).
[b] Predicted Caco-2 cell permeability in nm/s (acceptable range: <25 is poor, >500 is great).
[c] Predicted brain/blood partition coefficient (Concern value is −3.0 to −1.2).
[d] Predicted IC_{50} value for blockage of HERG K^+ channels (concern below −5).
[e] Predicted human oral absorption on 0–100% scale (acceptable range: <25% is poor, >80% is high).
[f] Predicted skin permeability, log K_p (acceptable range: −8.0 to −1.0).
[g] Number of likely metabolic reactions (acceptable range: 1–8).

*4.5.17. 4-((7-(4-bromophenoxy)-2-oxo-2H-chromene-3-carboxamido) methyl) benzoic acid (**6q**)*

Light brown solid; yield: 87%; mp: 258–260 °C; R_f = 0.35 (petroleum ether: ethyl acetate = 3:1)

IR (KBr): ν_{max} (cm^{-1}) 3346 (NH), 1705, 1652 and 1611 (CO); ^{1}H NMR (300 MHz, DMSO-d_6) δ 4.61 (t, 2H, J = 6.0Hz, CH_2), 5.26 (s, 2H, OCH_2), 7.07–7.20 (m, 2H, Ar-H), 7.20 (d, 1H, J = 2.1Hz, Ar-H), 7.44 (d, 2H, J = 6.9Hz, Ar-H), 7.61 (m, 3H, Ar-H), 7.91 (m, 3H, Ar-H), 8.85 (s, 1H, CH), 9.18 (t, 1H, J = 6.0Hz, NH), 13.00 (s, 1H, OH); ^{13}C NMR (75 MHz, DMSO-d_6) δ 42.98, 69.78, 101.65, 112.86, 114.52, 115.55, 121.85, 127.78, 129.83, 129.89, 130.58, 131.97, 132.10, 135.93, 144.79, 148.41, 156.53, 161.19, 162.21, 163.66, 167.63; Anal. calcd. for $C_{25}H_{18}BrNO_6$: C, 59.07; H, 3.57; N, 2.76; found: C 59.00, H 3.65, N 2.82.

*4.5.18. 4-((7-(4-methoxyphenoxy)-2-oxo-2H-chromene-3-carboxamido)methyl)benzoic acid (**6r**)*

Yellow solid; Yield: 82%; mp: 220–222 °C; R_f = 0.49 (petroleum ether: ethyl acetate = 3:1); IR (KBr): ν_{max} (cm^{-1}) 3342 (NH), 1701, 1659 and 1601 (CO); ^{1}H NMR (300 MHz, DMSO-d_6) δ 3.77 (s, 3H, CH_3), 4.62 (d, 2H, J = 6.0Hz, CH_2), 5.19 (s, 2H, CH_2), 6.97 (d, 2H, J = 8.4Hz, Ar-H), 7.10 (dd, 1H, J_1 = 8.7Hz, J_2 = 2.4Hz, Ar-H), 7.21 (d, 1H, J = 2.1Hz, Ar-H), 7.42–7.47 (m, 4H, Ar-H), 7.90 (m, 3H, Ar-H), 8.86 (s, 1H, CH), 9.17 (t, 3H, J = 6.0Hz, NH), 12.92 (S, 1H, OH); ^{13}C NMR (75 MHz, DMSO-d_6) δ 42.97, 55.60, 70.51, 101.61, 112.67, 114.40, 114.68, 115.34, 127.78, 128.27, 129.82, 129.90, 130.41, 132.06, 144.82, 148.47, 156.60, 159.75, 161.25, 162.24, 164.00, 167.63; Anal. calcd. for $C_{26}H_{21}NO_7$: C, 67.97; H, 4.61; N, 3.05; found: C 67.90, H 4.70, N 3.13.

*4.5.19. 4-((7-(2, 3-dichlorophenoxy)-2-oxo-2H-chromene-3-carboxamido) methyl) benzoic acid (**6s**)*

Pale yellow solid; yield: 85%; mp: 252–254 °C; R_f = 0.37 (petroleum ether: ethyl acetate = 3:1); IR (KBr): ν_{max} (cm^{-1}) 3358 (NH), 1704, 1654 and 1611 (CO); ^{1}H NMR (300 MHz, DMSO-d_6) δ 4.62 (t, 2H, J = 6.0 Hz,CH_2), 5.37 (s, 2H, OCH_2), 7.10–7.21 (m, 3H, Ar-H), 7.29 (d, 1H, J = 2.1Hz, Ar-H), 7.45 (d, 2H, J = 7.8Hz, Ar-H), 7.70 (m, 2H, Ar-H), 7.91 (m, 2H, Ar-H), 8.87 (s, 1H, CH), 9.19 (t, 1H, J = 6.0Hz, NH), 12.83 (brs, 1H, OH); ^{13}C NMR (75 MHz, DMSO-d_6) δ 42.98, 68.65, 101.71, 113.09, 114.41, 115.76, 127.79, 128.96, 129.45, 129.84, 129.90, 131.09, 131.42, 132.58, 136.45, 144.79, 148.38, 156.54, 161.17, 162.20, 163.48, 167.63; Anal. calcd. for $C_{25}H_{17}Cl_2NO_6$: C, 60.26; H, 3.44; N, 2.81; found: C 60.34, H 3.37, N 2.88.

*4.5.20. 4-((7-(2, 4-dichlorophenoxy)-2-oxo-2H-chromene-3-carboxamido) methyl) benzoic acid (**6t**)*

White solid; yield: 85%; mp: 245–247 °C; R_f = 0.38 (petroleum ether: ethyl acetate = 3:1); IR (KBr): ν_{max} (cm^{-1}) 3341 (NH), 1706, 1652 and 1600 (CO); ^{1}H NMR (300 MHz, DMSO-d_6) δ 4.62 (t, 2H, J = 6.0 Hz,CH_2), 5.32 (s, 2H, OCH_2), 7.5 (dd, 1H, J = 8.7Hz, J = 2.1Hz, Ar-H), 7.28 (d, 1H, J = 1.8Hz, Ar-H), 7.45 (d, 2H, J = 8.1Hz, Ar-H), 7.52 (dd, 1H, J = 8.1Hz, J = 1.8Hz, Ar-H), 7.68 (d, 1H, J = 8.4Hz, Ar-H), 7.74 (d, 1H, J = 2.1Hz, Ar-H), 7.86–7.97 (m, 3H, Ar-H), 8.87 (s, 1H, CH), 9.19 (t, 1H, J = 6.0Hz, NH), 12.88 (brs, 1H, OH); ^{13}C NMR (75 MHz, DMSO-d_6) δ 42.98, 67.78, 101.70, 113.06, 114.43, 115.74, 127.80, 128.15, 129.58, 129.74, 129.90, 131.09, 132.21, 132.45, 132.99, 134.56, 144.84, 148.39, 156.54, 161.17, 162.22, 163.51, 167.55; Anal. calcd. for $C_{25}H_{17}Cl_2NO_6$: C, 60.26; H, 3.44; N, 2.81; found: C 60.19, H 3.52, N 2.75.

*4.5.21. 4-((7-(3, 4-dichlorophenoxy)-2-oxo-2H-chromene-3-carboxamido) methyl) benzoic acid (**6u**)*

White solid; yield: 85%; mp: 249–251 °C; R_f = 0.53 (*n*-hexane: ethyl acetate = 3:1); IR (KBr): ν_{max} (cm^{-1}) 3353 (NH), 1705, 1656 and 1617 (CO); ^{1}H NMR (300 MHz, DMSO-d_6) δ(ppm) δ 4.61 (d, 2H, J = 6.0Hz, CH_2), 5.30 (s, 2H, OCH_2), 7.14 (dd, 1H, J_1 = 8.7Hz, J_2 = 2.4Hz, Ar-H), 7.23 (d, 1H, J = 2.1Hz, Ar-H), 7.44–7.52 (m, 3H, Ar-H), 7.69 (d, 1H, J = 8.1Hz, Ar-H), 7.79 (d, 1H, J = 1.8Hz, Ar-H), 7.93 (m, 3H, Ar-H), 8.86 (s, 1H, CH), 9.18 (t, 1H, J = 6.0Hz, NH), 12.92 (s, 1H,

OH); ^{13}C NMR (75 MHz, DMSO-d_6) δ 42.97, 69.01, 101.73, 112.99, 114.56, 115.70, 127.78, 128.64, 129.89, 130.31, 131.27, 131.30, 131.68,132.17, 137.70, 144.79, 148.38, 156.52, 161.17, 162.20, 163.45, 167.63; Anal. calcd. for $C_{25}H_{17}C_{l2}NO_6$: C, 60.26; H, 3.44; N, 2.81; found: C 60.20, H 3.45, N 2.91.

4.6. General procedure for the synthesis of N-(4-((2-aminophenyl) carbamoyl) benzyl)-2-oxo-2H-chromene-3-carboxamides (**8a-u**)

To a suspension of 4-((2-oxo-2H-chromene-3-carboxamido) methyl) benzoic acids (**6a-u**) (5 mmol) in dry THF (10 mL) was added CDI (19 mmol), and the mixture was stirred for 3 h at 60 °C. The clear solution was cooled to rt. To this solution were added 1, 2-phenylenediamine (**7**, 25 mmol) and TFA (1.2 mL) and then stirred for 16 h. The reaction mixture was evaporated to remove THF and the crude product was stirred in a mixture of hexane and water (2:5, v/v) for 1 h and filtered and dried. The residue was triturated in dichloromethane twice to afford pure compounds.

4.6.1. N-(4-((2-aminophenyl) carbamoyl) benzyl)-2-oxo-2H-chromene-3-carboxamide (**8a**)

White solid; yield: 90%; mp: 207–209 °C; $R_f = 0.76$ (petroleum ether: ethyl acetate = 3:2); IR (KBr): ν_{max} (cm^{-1}) 3404 and 3322 (NH and NH_2), 1720, 1653 and 1609 (CO); ^{1}H NMR (300 MHz, DMSO-d_6) δ 4.64 (d, 2H, J = 6.0 Hz, CH_2), 4.90 (s, 2H, NH_2, D_2O exchangable), 6.62 (t, 1H, J = 6.6 Hz, Ar-H), 6.79 (d, 1H, J = 7.5 Hz, Ar-H), 6.93 (t, 1H, J = 7.5 Hz, Ar-H), 7.18 (d, 1H, J = 6.0 Hz, Ar-H), 7.48–7.55 (m, 4H, Ar-H), 7.75 (t, 1H, J = 6.0 Hz, Ar-H), 7.98 (m, 2H, Ar-H), 8.90 (s, 1H, CH), 9.22 (t, 1H, J = 6.0 Hz, NH, D_2O exchangable), 9.64 (s, 1H, NH, D_2O exchangable); ^{13}C NMR (75 MHz, DMSO-d_6) δ 43.03, 116.63, 116.79, 118.95, 119.58, 123.70, 125.63, 126.93, 127.05, 127.63, 128.36, 129.93, 130.75, 133.75, 134.62, 143.00, 148.05, 154.39, 160.78, 161.91, 165.53; LCMS(ESI, m/z): $(M+1)^+$ 414.0, $[2\ M + 1]^+$ 827.2; Anal. calcd. for $C_{24}H_{19}N_3O_4$: C, 69.72; H, 4.63; N, 10.16; found: C 69.78, H 4.69, N 10.06.

4.6.2. N-(4-((2-aminophenyl) carbamoyl) benzyl)-8-methoxy-2-oxo-2H-chromene-3-carboxamide (**8b**)

White solid; yield: 80%; mp: 213–215 °C; $R_f = 0.65$ (petroleum ether: ethyl acetate = 3:2); IR (KBr): ν_{max} (cm^{-1}) 3402 and 3342 (NH and NH_2), 1701, 1659 and 1601 (CO); ^{1}H NMR (300 MHz, DMSO-d_6) δ 3.95 (s, 3H, OCH_3), 4.58 (d, 2H, J = 6.0 Hz, CH_2), 4.95 (s, 2H, NH_2),6.64 (t, 1H, J = 6.0 Hz, Ar-H), 6.79 (d, 1H, J = 6.6 Hz, Ar-H), 6.97 (t, 1H, J = 6.6 Hz, Ar-H), 7.15 (d, 1H, J = 6.6 Hz, Ar-H), 7.30–7.50 (m, 5H, Ar-H), 7.95 (d, 2H, J = 6.6 Hz, Ar-H), 8.87 (s, 1H, CH), 9.23 (t, 2H, J = 6.0 Hz, NH), 9.66 (s, 1H, NH); ^{13}C NMR (75 MHz, DMSO-d_6) δ 43.04, 56.69, 116.59, 116.80, 119.51, 119.70, 121.66, 123.71, 125.58, 126.93, 127.04, 127.66, 128.36, 133.76, 142.99, 143.41, 143.72, 146.77, 148.27, 160.49, 161.88, 161.93, 165.59; LCMS(ESI, m/z): $[M+1]^+$ 444.0, $(2\ M + 1)^+$ 887.3; Anal. calcd. for $C_{25}H_{21}N_3O_5$: C, 67.71; H, 4.77; N, 9.48; found: C 67.82, H 4.82, N 9.56.

4.6.3. N-(4-((2-aminophenyl) carbamoyl) benzyl)-8-ethoxy-2-oxo-2H-chromene-3-carboxamide (**8c**)

White solid; yield: 87%; mp: 218–220 °C; $R_f = 0.46$ (petroleum ether: ethyl acetate = 3:2); IR (KBr): ν_{max} (cm^{-1}) 3400 and 3326 (NH and NH_2), 1720, 1653 and 1613 (CO); ^{1}H NMR (300 MHz, DMSO-d_6) δ 1.43 (t, 3H, J = 6.9 Hz, CH_3), 4.23 (q, 2H, J = 6.9 Hz, OCH_2), 4.63 (s, 2H, J = 5.4 Hz, CH_2), 4.92 (s, 2H, NH_2), 6.61 (t, 1H, J = 6.9 Hz, Ar-H), 6.78 (d, 1H, J = 6.9 Hz, Ar-H), 7.00 (t, 1H, J = 6.9 Hz, Ar-H), 7.17 (d, 1H, J = 7.2 Hz, Ar-H), 7.33–7.54 (m, 5H, Ar-H), 7.95 (d, 2H, J = 8.1 Hz, Ar-H), 8.87 (s, 1H, CH), 9.24 (t, 1H, J = 6.0 Hz, NH), 9.66 (s, 1H, NH); ^{13}C NMR (75 MHz, DMSO-d_6) δ 15,04, 43.01, 65.00, 116.56, 116.74, 117.37, 119.60, 121.61, 123.65, 123.76, 125.58, 126.95, 127.15, 127.65, 128.36, 133.76, 143.00, 143.50, 143.76, 145.98, 148.35, 160.57, 161.90, 165.61; LCMS(ESI, m/z): 458.0 $[M+1]^+$, 915.1 $[2\ M + 1]^+$; Anal. calcd. for $C_{26}H_{23}N_3O_5$: C, 68.41; H, 5.07; N, 9.19; found: C 68.29, H 5.01, N 9.05.

4.6.4. N-(4-((2-aminophenyl)carbamoyl)benzyl)-7-methoxy-2-oxo-2H-chromene-3- carboxamide (**8d**)

Yellow solid; yield: 92%; mp: 212–214 °C; $R_f = 0.53$ (petroleum ether: ethyl acetate = 3:2); IR (KBr): ν_{max} (cm^{-1}) 3402 and 3342 (NH and NH_2), 1701, 1659 and 1601 (CO); ^{1}H NMR (300 MHz, DMSO-d_6) δ 3.91 (s, 3H, OCH_3), 4.62 (d, 2H, J = 5.4Hz, CH_2), 4.94 (brs, 2H, NH_2), 6.61 (t, 1H, J = 7.2Hz, Ar-H), 6.78 (d, 1H, J = 7.8Hz, Ar-H), 7.00 (t, 1H, J = 7.2Hz, Ar-H), 7.05 (m, 3H, Ar-H), 7.48 (d, 2H, J = 8.4Hz, Ar-H), 7.95 (m, 3H, Ar-H), 8.87 (s, 1H, CH), 9.19 (t, 1H, J = 5.4Hz, NH), 9.66 (s, 1H, NH); ^{13}C NMR (75 MHz, DMSO-d_6) δ 42.85, 56.75, 100.78, 112.62, 114.14, 115.32, 116.59, 116.79, 123.68, 126.95, 127.07, 127.61, 128.36, 132.07, 133.70, 143.12, 143.42, 148.48, 156.70, 161.26, 162.19, 164.94, 165.53; LCMS(ESI, m/z): 444.0 $[M+1]^+$, 887.3 $[2\ M + 1]^+$; Anal. calcd. for $C_{25}H_{21}N_3O_5$: C, 67.71; H, 4.77; N, 9.48; found: C 67.86, H 4.63, N 9.59.

4.6.5. N-(4-((2-aminophenyl) carbamoyl) benzyl)-7-ethoxy-2-oxo-2H-chromene-3-carboxamide (**8e**)

Yellow solid; yield: 87%; mp: 224–226 °C; $R_f = 0.53$ (petroleum ether: ethyl acetate = 3:2); IR (KBr): ν_{max} (cm^{-1}) 3409 and 3330 (NH and NH_2), 1714, 1653 and 1614 (CO); ^{1}H NMR (300 MHz, DMSO-d_6) δ 1.38 (t, 3H, J = 6.3Hz, CH_3), 4.18 (q, 2H, J = 6.6Hz, OCH_2), 4.62 (d, 2H, J = 4.8Hz, $2CH_2$), 4.99 (brs, 2H, NH_2), 6.61 (t, 1H, J = 6.6Hz, Ar-H), 6.93–6.7.19 (m, 5H, Ar-H), 7.47 (d, 2H, J = 7.8Hz, Ar-H), 7.94 (m, 3H, Ar-H), 8.87 (s, 1H, CH), 9.18 (t, 1H, J = 7.8 Hz, NH), 9.66 (s, 1H, NH); ^{13}C NMR (75 MHz, DMSO-d_6) δ 14.81, 42.97, 64.90, 101.11, 112.51, 114.38, 115.21, 116.56, 116.74, 123.66, 126.94, 127.08, 127.61, 128.36, 132.08, 133.71, 143.13, 143.54,148.49, 156.70, 161.32, 162.19, 164.21, 165.60; LCMS(ESI, m/z): 458.1 $[M+1]^+$, 915.1 $[2\ M + 1]^+$; Anal. calcd. for $C_{26}H_{23}N_3O_5$: C, 68.26; H, 5.07; N, 9.19; found: C 68.10, H 5.17, N 9.31.

4.6.6. N-(4-((2-aminophenyl) carbamoyl) benzyl)-2-oxo-7-propoxy-2H-chromene-3-carboxamide (**8f**)

Yellow solid; yield: 89%; mp: 219–221 °C; $R_f = 0.54$ (petroleum ether: ethyl acetate = 3:2); IR (KBr): ν_{max} (cm^{-1}) 3403 and 3335 (NH and NH_2), 1706, 1652 and 1618 (CO); ^{1}H NMR (300 MHz, DMSO-d_6) δ 1.00 (t, 3H, J = 7.2Hz, CH_3), 1.79 (se, 2H, J = 6.9Hz, CH_2), 4.10 (t, 2H, J = 6.6Hz, OCH_2), 4.62 (d, 2H, J = 5.7Hz, CH_2), 4.89 (s, 2H, NH_2), 6.61 (t, 1H, J = 7.8Hz, Ar-H), 6.78 (d, 1H, J = 6.9Hz, Ar-H), 6.96 (d, 2H, J = 8.7Hz, Ar-H), 7.12 (d, 1H, J = 7.5Hz, Ar-H), 7.18 (d, 1H, J = 7.5Hz, Ar-H), 7.46 (d, 2H, J = 8.1Hz, Ar-H), 7.90–7.97 (m, 3H, Ar-H), 8.87 (s, 1H, CH), 9.18 (t, 1H, J = 6.0Hz, NH), 9.66 (s, 1H, NH); ^{13}C NMR (75 MHz, DMSO-d_6) δ 10.75, 22.24, 42.85, 70.57, 101.17, 112.52, 114.42, 115.21, 116.58, 116.78, 123.69, 126.93, 127.05, 127.61, 128.36, 132.09, 133.72, 143.11, 148.49, 156.71,161.30, 162.12, 164.39, 165.58; LCMS(ESI, m/z): 472.0 $[M+1]^+$, 943.3 $[2\ M + 1]$; Anal. calcd. for $C_{27}H_{25}N_3O_5$: C, 68.78; H, 5.34; N, 8.91; found: C 68.89, H 5.22, N 8.80.

4.6.7. N-(4-((2-aminophenyl) carbamoyl) benzyl)-6-bromo-2-oxo-2H-chromene-3-carboxamide (**8g**)

White solid; yield: 90%; mp: 283–285 °C; $R_f = 0.53$ (*n*-hexane: ethyl acetate = 3:2); IR (KBr): ν_{max} (cm^{-1}) 3402 and 3343 (NH and NH_2), 1714, 1653 and 1611 (CO); ^{1}H NMR (300 MHz, DMSO-d_6) δ 4.62 (d, 2H, J = 5.7Hz, CH_2), 5.07 (brs, 2H, NH_2), 6.61 (t, 1H, J = 7.2Hz, Ar-H), 6.79 (d, 1H, J = 7.5Hz, Ar-H), 6.98 (t, 1H, J = 7.2Hz, Ar-H), 7.17 (d, 1H, J = 7.8Hz, Ar-H), 7.47–7.52 (m, 3H, Ar-H), 7.88–7.98 (m, 3H, Ar-H), 8.26 (d, 1H, J = 2.1Hz, Ar-H), 8.85 (s, 1H, CH), 9.21 (t, 1H, J = 6.0Hz, NH), 9.66 (s, 1H, NH); ^{13}C NMR (75 MHz, DMSO-d_6) δ 42.94, 116.62, 116.84, 117.12, 118.91, 123.70, 126.96,

127.07, 127.62, 128.35, 129.92, 130.10, 132.57, 133.72, 136.74, 142.92, 143.38, 146.70, 155.63, 160.26, 161.54, 165.54; LCMS(ESI, *m*/*z*): 493.7 $[M+1]^+$; Anal. calcd. for $C_{24}H_{18}BrN_3O_4$: C, 58.55; H, 3.69; N, 8.54; found: C 58.67, H 3.80, N 8.61.

*4.6.8. N-(4-((2-aminophenyl) carbamoyl) benzyl)-7-(benzyloxy)-2-oxo-2H-chromene-3-carboxamide (**8h**)*

White solid; yield: 80%; mp: 212–214 °C; $R_f = 0.58$ (petroleum ether: ethyl acetate = 3:2); IR (KBr): ν_{max} (cm^{-1}) 3407 and 3332 (NH and NH_2), 1703, 1656 and 1612 (CO); ^1H NMR (300 MHz, DMSO-d_6) δ 4.63 (d, 2H, $J = 5.7$Hz, CH_2), 4.90 (brs, 2H, NH_2), 5.28 (s, 2H, OCH_2),6.61 (t, 1H, $J = 7.2$Hz, Ar-H), 6.80 (d, 1H, $J = 7.2$, Ar-H), 7.01 (t, 1H, $J = 7.2$Hz, Ar-H), 7.12–7.22 (m, 3H, Ar-H), 7.39–7.51 (m, 7H, Ar-H), 7.95 (m,3H, Ar-H), 8.87 (s, 1H, CH), 9.18 (t, 1H, $J = 6.0$Hz, NH), 9.66 (s, 1H, NH); ^{13}C NMR (75 MHz, DMSO-d_6) δ 42.98, 70.68, 101.66, 112.78, 114.65, 115.50, 116.59, 116.77, 123.68, 123.79, 126.94, 127.06, 127.62, 128.50, 128.71, 129.04, 129.97, 132.11, 136.44, 143.12, 143.49, 148.40, 156.57, 161.26, 162.18, 163.90, 165.55; LCMS(ESI, *m*/*z*): 542.0 $[M+23]^+$, 1062.2 $[2\ M + 23]^+$, 1581.0 $[3\ M + 23]^+$; Anal. calcd. for $C_{31}H_{25}N_3O_5$: C, 71.66; H, 4.85; N, 8.09; found: C, 71.49, H, 5.01, N, 7.92.

*4.6.9. N-(4-((2-aminophenyl) carbamoyl) benzyl)-7-((2-methylbenzyl) oxy)-2-oxo-2H-chromene-3-carboxamide (**8i**)*

White solid; Yield: 86%; mp: 207–209 °C; $R_f = 0.62$ (petroleum ether: ethyl acetate = 3:2); IR (KBr): ν_{max} (cm^{-1}) 3409 and 3335 (NH and NH_2), 3052, 2926 (CH_2) 1704, 1658 and 1616 (CO); ^1H NMR (300 MHz, DMSO-d_6) δ 2.35 (s, 3H, CH_3), 4.63 (d, 2H, $J = 5.7$Hz, CH_2), 4.93 (brs, 2H, NH_2), 5.27 (s, 2H, OCH_2), 6.61 (t, 1H, $J = 6.9$Hz, Ar-H), 6.87 (d, 1H, $J = 6.9$Hz, Ar-H), 6.98 (t, 1H, $J = 6.9$Hz, Ar-H) 7.13–7.21 (m, 2H, Ar-H), 7.23–7.29 (m, 4H, Ar-H 7.45–7.50 (m, 3H, Ar-H), 7.93–7.99 (m, 3H, Ar-H), 8.88 (s, 1H, CH), 9.19 (t, 1H, $J = 6.0$Hz, NH), 9.67 (s, 1H, NH); ^{13}C NMR (75 MHz, DMSO-d_6) δ 18.96, 42.99, 69.46, 101.63, 112.81, 114.60, 115.47, 116.58, 172.73, 123.79, 126.58, 126.94, 127.15, 127.63, 128.37, 128.95, 129.32, 130.74, 132.12, 133.78, 134.38, 137.36, 143.11, 143.59, 148.43, 156.62, 161.28, 162.17, 164.03, 165.60; LCMS(ESI, *m*/*z*): 534.1 $[M+1]^+$; Anal. calcd. for $C_{32}H_{27}N_3O_5$: C, 72.03; H, 5.10; N, 7.88; found: C, 72.15; H 5.28; N, 7.71.

*4.6.10. N-(4-((2-aminophenyl) carbamoyl) benzyl)-7-((3-methylbenzyl) oxy)-2-oxo-2H-chromene-3-carboxamide (**8j**)*

White solid; Yield: 88%; mp: 213–215 °C; $R_f = 0.52$ (petroleum ether: ethyl acetate = 3:2); IR (KBr): ν_{max} (cm^{-1}) 3402 and 3340 (NH and NH_2), 1704, 1658 and 1602 (CO); ^1H NMR (300 MHz, DMSO-d_6) δ 2.34 (s, 3H, CH_3), 4.62 (d, 2H, $J = 5.7$Hz, CH_2), 4.95 (brs, 2H, NH2), 5.23 (s, 1H, OCH_2), 6.61 (t, 1H, $J = 7.5$Hz, Ar), 6.80 (d, 1H, $J = 7.5$Hz, Ar-H), 6.96 (t, 1H, $J = 8.1$Hz, Ar-H), 7.00–7.21 (m, 4H, Ar-H), 7.29–7.34 (m, 3H, Ar-H), 7.47 (d, 2H, $J = 8.1$Hz, Ar-H), 7.95 (m, 3H, Ar-H), 8.87 (s, 1H, CH), 9.18 (t, 1H, $J = 5.7$Hz, NH), 9.66 (s, 1H, NH); ^{13}C NMR (75 MHz, DMSO-d_6) δ 21.44, 42.98, 70.72, 101.61, 112.75, 114.64, 115.45, 116.60, 116.76, 123.78, 125.59, 126.97, 127.16, 127.62, 128.36, 128.95, 129.34, 130.10, 132.10, 133.74, 136.33, 138.26, 143.11, 143.57, 148.41, 156.57, 161.27, 162.19, 163.93, 165.63; LCMS(ESI): 533.9 $[M+1]^+$; Anal. calcd. for $C_{32}H_{27}N_3O_5$: C, 72.03; H, 5.10; N, 7.88; found: C, 71.89; H, 5.25; N, 8.01.

*4.6.11. N-(4-((2-aminophenyl) carbamoyl) benzyl)-7-((4-methylbenzyl) oxy)-2-oxo-2H-chromene-3-carboxamide (**8k**)*

White solid; Yield: 90%, mp: 221–223 °C; $R_f = 0.53$ (petroleum ether: ethyl acetate = 3:2); IR (KBr): ν_{max} (cm^{-1}) 3404 and 3345 (NH and NH_2), 3030, 2921 (CH_2), 1707, 1655 and 1608 (CO), 1565, 1525, 1450, 1224, 1147, 822, 741; ^1H NMR (300 MHz, DMSO-d_6) δ 2.32 (s, 3H, CH_3), 4.62 (d, 2H, $J = 6.0$Hz, CH_2), 4.90 (brs, 2H, NH_2), 5.22 (s, 2H, CH_2), 6.61 (t, 1H, $J = 7.2$Hz, Ar-H), 6.80 (d, 1H, $J = 6.9$Hz, Ar-H), 6.98 (t, 1H, $J = 7.2$Hz, Ar-H) 7.12–7.24 (m, 5H, Ar-H), 7.37 (d, 2H, $J = 7.8$Hz, Ar-H), 7.46 (d, 2H, $J = 8.1$Hz, Ar-H), 7.94 (m, 3H, Ar-H), 8.86 (s, 1H, CH), 9.18 (t, 1H, $J = 6.0$Hz, NH), 9.66 (s, 1H, NH); ^{13}C NMR (400 MHz, DMSO-d_6) δ 21.26, 42.97, 70.59, 101.63, 112.70, 114.69, 115.40, 116.60, 116.77, 123.76, 126.98, 127.16, 127.62, 128.36, 128.60, 129.68, 132.08, 133.37, 133.73, 138.05, 143.11, 143.57, 148.42, 156.56, 161.27, 162.20, 163.93, 165.94; LCMS(ESI, *m*/*z*): 556.1 $[M+23]^+$, 1089.2 $[2\ M + 23]^+$; Anal. calcd. for $C_{32}H_{27}N_3O_5$: C, 72.03; H, 5.10; N, 7.88; found: C, 72.23; H, 4.91; N, 8.09.

*4.6.12. N-(4-((2-aminophenyl) carbamoyl) benzyl)-7-((2-fluorobenzyl) oxy)-2-oxo-2H-chromene-3-carboxamide (**8l**)*

White solid; yield: 86%; mp: 215–217 °C; $R_f = 0.67$ (petroleum ether: ethyl acetate = 3:2); IR (KBr): ν_{max} (cm^{-1}) 3401 and 3354 (NH and NH_2), 1718, 1654 and 1616 (CO); ^1H NMR (300 MHz, DMSO-d_6) δ 4.63 (d, 2H, $J_2 = 5.7$Hz, CH_2), 5.04 (brs, 2H, NH_2), 5.32 (s, 2H, OCH_2), 6.61 (t, 1H, $J_2 = 7.2$Hz, Ar-H), 6.78 (d, 1H, $J_2 = 8.1$Hz, Ar-H), 6.98 (t, 1H, $J_2 = 6.9$Hz, Ar-H), 7.13–7.20 (m, 2H, Ar-H), 7.25–7.33 (m, 3H, Ar-H), 7.47 (m, 3H, Ar-H), 7.62 (t, 1H, $J_2 = 7.5$Hz, Ar-H), 7.94–8.00 (m, 3H, Ar-H), 8.88 (s, 1H, CH), 9.18 (t, 1H, $J_2 = 6.0$Hz, Ar), 9.65 (s, 1H, NH); ^{13}C NMR (75 MHz, DMSO-d_6) δ 43.00, 65.13, 101.57, 112.91, 114.47, 115.61, 115.86, 116.64, 116.82, 123.32, 123.80, 125.15, 1126.99, 127.63, 128.37, 130.09, 131.48, 131.57, 131.62, 132.15, 143.10, 143.55, 148.37, 156.55, 159.40, 161.25, 162.19, 163.68, 165.68; LCMS(ESI, *m*/*z*): 538.0 $[M+1]^+$; Anal. calcd. for $C_{31}H_{24}FN_3O_5$: C, 69.27; H, 4.50; N, 7.82; found: C, 69.15; H, 4.37; N, 7.70.

*4.6.13. N-(4-((2-aminophenyl) carbamoyl) benzyl)-7-((3-fluorobenzyl) oxy)-2-oxo-2H-chromene-3-carboxamide (**8m**)*

White solid; yield: 88%; mp: 208–210 °C; $R_f = 0.65$ (petroleum ether: ethyl acetate = 3:2)

IR (KBr): ν_{max} (cm^{-1}) 3409 and 3340 (NH and NH_2), 1704, 1658 and1602 (CO); ^1H NMR (300 MHz, DMSO-d_6) δ 4.62 (d, 2H, $J_2 = 5.7$Hz, CH_2), 4.93 (brs, 2H, NH_2), 5.31 (s, 2H, OCH_2), 6.61 (t, 1H, $J = 7.5$Hz, Ar-H), 6.78 (d, 1H, $J = 7.8$Hz, Ar-H), 7.00 (t, 1H, $J_2 = 8.1$Hz, Ar-H), 7.13–7.24 (m, 4H, Ar-H), 7.33 (d, 2H, $J = 8.1$Hz, Ar-H), 7.44–7.52 (m, 3H, Ar-H), 7.93–7.98 (m, 3H, Ar-H), 8.88 (s, 1H, CH), 9.19 (t, 1H, $J_2 = 6.0$Hz, Ar), 9.66 (s, 1H, NH); ^{13}C NMR (75 MHz, DMSO-d_6) δ 43.00, 69.74, 101.69, 112.90, 114.57, 114.88, 115.59, 116.60, 116.75, 123.80, 124.32, 126.96, 127.16, 127.62, 128.37, 130.12, 131.15, 132.13, 133.76, 139.28, 143.10, 143.59, 148.36, 156.52, 161.24, 162.15, 163.62, 164.28, 165.62; LCMS(ESI, *m*/*z*): 538.0 $[M+1]^+$; Anal. calcd. for $C_{31}H_{24}FN_3O_5$: C, 69.27; H, 4.50; N, 7.82; found: C, 69.37; H, 4.49; N, 7.72.

*4.6.14. N-(4-((2-aminophenyl) carbamoyl) benzyl)-7-((4-fluorobenzyl) oxy)-2-oxo-2H-chromene-3-carboxamide (**8n**)*

White solid; yield: 86%; mp: 212–214 °C; $R_f = 0.67$ (petroleum ether: ethyl acetate = 3:2); IR (KBr): ν_{max} (cm^{-1}) 3403 and 3346 (NH and NH_2), 1707, 1656 and 1608 (CO); ^1H NMR (300 MHz, DMSO-d_6) δ 4.62 (d, 2H, $J_2 = 5.7$Hz, CH_2), 4.92 (brs, 2H, NH_2), 5.26 (s, 2H, OCH_2), 6.62 (t, 1H, $J_2 = 7.2$Hz, Ar-H), 6.80 (d, 1H, $J_2 = 6.9$Hz, Ar-H), 6.96 (t, 1H, $J_2 = 6.9$Hz, Ar-H), 7.11–7.30 (m, 5H, Ar-H), 7.49 (d, 2H, $J_2 = 8.1$Hz, Ar-H), 7.54–7.60 (mt, 2H, Ar-H), 7.95 (m, 3H, Ar-H), 8.87 (s, 1H, CH), 9.18 (t, 1H, $J_2 = 6.0$Hz, Ar), 9.67 (s, 1H, NH); ^{13}C NMR (75 MHz, DMSO-d_6) δ 42.99, 69.94, 101.66, 112.82, 114.61, 115.54, 116.06, 116.60, 116.79, 123.81, 126.94, 127.12, 127.62, 128.36, 129.98, 130.12, 130.81, 132.11, 132.67, 133.73, 136.37, 143.11, 143.44, 148.39, 156.56, 161.25, 162.17, 163.78, 165.63; LCMS(ESI; *m*/*z*): 561.0 $[M+23]^+$, 1097.1 $[2\ M + 23]^+$, 1635.5 $[3\ M + 23]^+$; Anal. calcd. for $C_{31}H_{24}FN_3O_5$: C, 69.27; H, 4.50; N, 7.82; found: C, 69.39; H, 4.39; N, 7.70.

*4.6.15. N-(4-((2-aminophenyl) carbamoyl) benzyl)-7-((2-chlorobenzyl)oxy)-2-oxo-2H-chromene-3-carboxamide (**8o**)*

Yellow solid; yield: 87%; mp: 223–225 °C; $R_f = 0.56$ (petroleum

ether: ethyl acetate = 3:2); IR (KBr): ν_{max} (cm^{-1}) 3401 and 3340 (NH and NH_2), 1710, 1654 and 1615 (CO); ^1H NMR (300 MHz, DMSO-d_6) δ 4.62 (d, 2H, J = 6.0, CH_2), 4.95 (brs, 2H, NH_2), 5.28 (s, 2H, OCH_2), 6.61 (t, 1H, J = 7.2, Ar-H), 6.80 (d, 1H, J = 7.2, Ar-H), 6.95 (t, 1H, J = 8.4, Ar-H), 7.01 (d, 1H, J = 8.1, Ar-H), 7.11–7.22 (m, 3H, Ar-H), 7.49–7.55 (m, 5H, Ar-H), 7.95 (m, 3H, Ar-H), 8.87 (s, 1H, CH), 9.18 (t, 1H, J = 6.0Hz, NH), 9.66 (s, 1H, NH); ^{13}C NMR (75 MHz, DMSO-d_6) δ 42.98, 68.43, 101.63, 112.98, 114.46, 115.67, 116.59, 116.77, 123.77, 126.97, 127.15, 127.63, 127.99, 128.37, 130.04, 130.10, 13.92, 131.30, 132.20, 133.20, 133.72, 143.12, 143.55, 148.38, 156.57, 161.24, 162.118, 163.70, 165.57; LCMS(ESI, m/z): 576.2 $[M+23]^+$, 1129.1 $[2\ M + 23]^+$, 1681.5 $[3\ M + 23]^+$; Anal. calcd. for $C_{31}H_{24}ClN_3O_5$: C, 67.21; H, 4.37; N, 7.58; found: C, 67.09; H, 4.44; N, 7.49.

4.6.16. N-(4-((2-aminophenyl) carbamoyl) benzyl)-7-((4-chlorobenzyl) oxy)-2-oxo-2H-chromene-3-carboxamide (**8p**)

Yellow solid; yield: 87%; mp: 220–222 °C; R_f = 0.66 (petroleum ether: ethyl acetate = 3:2); IR (KBr): ν_{max} (cm^{-1}) 3401 and 3344 (NH and NH_2), 1704, 1658 and 1611 (CO); ^1H NMR (300 MHz, DMSO-d_6) δ 4.62 (d, 2H, J = 6.0, CH_2), 4.95 (brs, 2H, NH_2), 5.28 (s, 2H, OCH_2), 6.61 (t, 1H, J = 7.2, Ar-H), 6.80 (d, 1H, J = 7.2, Ar-H), 6.95 (t, 1H, J = 8.4, Ar-H), 7.01 (d, 1H, J = 8.1, Ar-H), 7.11–7.22 (m, 3H, Ar-H), 7.49–7.55 (m, 5H, Ar-H), 7.95 (m, 3H, Ar-H), 8.87 (s, 1H, CH), 9.18 (t, 1H, J = 6.0Hz, NH), 9.66 (s, 1H, NH); ^{13}C NMR (75 MHz, DMSO-d_6) δ 43.00, 69.77, 101.66, 112.86, 114.58, 115.53, 116.62, 116.77, 123.81, 126.96, 127.17, 127.62, 128.38, 129.04, 130.12, 132.11, 133.31, 133.76, 135.47, 143.10, 143.57, 148.37, 156.52, 161.24, 162.15, 163.66, 165.63; LCMS(ESI, m/z): 554.1 $[M+1]^+$; Anal. calcd. for $C_{31}H_{24}ClN_3O_5$: C, 67.21; H, 4.37; N, 7.58; found: C, 67.10; H, 4.49; N, 7.43.

4.6.17. N-(4-((2-aminophenyl) carbamoyl) benzyl)-7-((4-bromobenzyl) oxy)-2-oxo-2H-chromene-3-carboxamide (**8q**)

White solid; yield: 90%; mp: 200–202 °C; R_f = 0.58 (petroleum ether: ethyl acetate = 3:2); IR (KBr): ν_{max} (cm^{-1}) 3400 and 3321 (NH and NH_2), 1690, 1653 and 1616 (CO); ^1H NMR (300 MHz, DMSO-d_6) δ 4.62 (d, 3H, J = 6.0Hz, CH_2), 4.93 (brs, 2H, NH_2), 5.27 (s, 2H, OCH_2), 6.63 (t, 1H, J = 7.2Hz, Ar-H), 6.82 (d, 1H, J = 7.8Hz, Ar-H), 6.95 (t, 1H, J = 7.8Hz, Ar-H), 7.10–7.20 (m, 3H, Ar-H), 7.48 (m, 3H, Ar-H), 7.61–7.65 (m, 3H, Ar-H), 7.92–7.99 (m, 3H, Ar-H), 8.87 (s, 1H, CH), 9.18 (t, 1H, J = 6.0Hz, NH), 9.66 (s, 1H, NH); ^{13}C NMR (75 MHz, DMSO-d_6) δ 42.99, 69.81, 101.68, 112.87, 114.59, 115.55, 116.60, 116.75, 121.82, 123.80, 126.95, 127.15, 127.62, 128.37, 129.37, 130.57, 132.11, 133.77, 135.90,143.09, 148.37, 156.52, 161.23, 162.14, 163.65, 165.62; LCMS(ESI, m/z): 597.9 $[M]^+$; Anal. calcd. for $C_{31}H_{24}BrN_3O_5$: C, 62.22; H, 4.04; N, 7.02; found: C, 62.31; H, 4.12; N, 7.11.

4.6.18. N-(4-((2-aminophenyl) carbamoyl) benzyl)-7-((4-methoxybenzyl)oxy)-2-oxo-2H-chromene-3-carboxamide (**8r**)

Pale brown solid; Yield: 90%; mp: 202–204 °C; R_f = 0.64 (petroleum ether: ethyl acetate = 3:2); IR (KBr): ν_{max} (cm^{-1}) 3405 and 3344 (NH and NH_2), 1709, 1653 and 1616 (C=O); ^1H NMR (300 MHz, DMSO-d_6) δ 3.77 (s, 3H, CH_3), 4.63 (d, 2H, J = 6.0Hz, CH_2), 4.93 (brs, 2H, NH_2), 5.19 (s, 1H, OCH_2), 6.61 (t, 1H, J = 7.2Hz, Ar-H), 6.80 (d, 1H, J = 7.2Hz, Ar-H), 6.96–7.01 (m, 3H, Ar-H), 7.12 (dd, 1H, J_1 = 8.7Hz, J_2 = 2.1Hz, Ar-H), 7.16–7.22 (m, 2H, Ar-H), 7.42–7.49 (m, 4H, Ar-H), 7.91–7.98 (m, 3H, Ar-H), 8.87 (s, 1H, CH), 9.18 (t, 1H, J = 6.0Hz, NH), 9.66 (s, 1H, NH); ^{13}C NMR (75 MHz, DMSO-d_6) δ 42.98, 55.58, 70.51, 101.59, 112.65, 114.39, 114.69, 115.32, 116.62, 116.80, 123.78, 126.99, 127.16, 127.63, 128.24, 130.39, 132.05, 133.73, 143.11, 143.56, 148.43, 156.57, 159.74, 161.29, 162.21, 163.99, 165.66; LCMS(ESI, m/z): 550.0 $(M+1)^+$; Anal. calcd. for $C_{32}H_{27}N_3O_6$: C, 69.93; H, 4.95; N, 7.65; found: C, 69.83; H, 5.06; N, 7.54.

4.6.19. N-(4-((2-aminophenyl) carbamoyl) benzyl)-7-((2,3-dichlorobenzyl)oxy)-2-oxo-2H-chromene-3-carboxamide (**8s**)

White solid; yield: 88%; mp: 221–223 °C; R_f = 0.63 (petroleum ether: ethyl acetate = 3:2); IR (KBr): ν_{max} (cm^{-1}) 3409 and 3358 (NH and NH2), 1704, 1658 and 1611 (CO); ^1H NMR (300 MHz, DMSO-d_6) δ 4.62 (d, 2H, J_2 = 5.7Hz, CH_2), 4.91 (brs, 2H, NH_2), 5.39 (s, 2H, OCH_2), 6.60 (t, 1H, J_2 = 7.5Hz, Ar-H), 6.80 (d, 1H, J_2 = 8.1Hz, Ar-H), 7.00 (t, 1H, J_2 = 8.1Hz, Ar-H), 7.15–7.21 (m, 2H, Ar-H), 7.30 (d, 1H, J_2 = 2.4Hz, Ar-H), 7.43–7.7.50 (m, 3H, Ar-H), 7.66 (d, 1H, J_2 = 7.8Hz, Ar-H), 7.72 (d, 1H, J_2 = 7.8Hz, Ar-H), 7.94–8.02 (m, 3H, Ar-H), 8.88 (s, 1H, CH), 9.18 (t, 1H, J_2 = 6.0Hz, Ar-H), 9.65 (s, 1H, NH); ^{13}C NMR (75 MHz, DMSO-d_6) δ 42.99, 68.69, 101.75, 113.11, 114.41, 115.82, 116.57, 116.72, 123.78, 126.97, 127.15, 127.62, 128.36, 128.97, 129.48, 131.11, 131.44, 132.23, 133.77, 136.45, 143.10, 143.59, 148.34, 156.53, 161.20, 162.14, 163.48, 165.60; LCMS(ESI, m/z): 588.2 $[M]^+$; Anal. calcd. for $C_{31}H_{23}Cl_2N_3O_5$: C, 63.27; H, 3.94; Cl, 12.05; N, 7.14; found: C, 63.14; H, 3.84; N, 7.03.

4.6.20. N-(4-((2-aminophenyl) carbamoyl) benzyl)-7-((2,4-dichlorobenzyl)oxy)-2-oxo-2H-chromene-3-carboxamide (**8t**)

White solid; yield: 88%; mp: 200–202 °C; R_f = 0.63 (petroleum ether: ethyl acetate = 3:2); IR (KBr): ν_{max} (cm^{-1}) 3405 and 3352 (NH and NH_2), 1705, 1656 and 1614 (CO); ^1H NMR (300 MHz, DMSO-d_6) δ 4.62 (d, 2H, J_2 = 5.7Hz, CH_2), 4.90 (brs, 2H, NH_2), 5.32 (s, 2H, OCH_2), 6.61 (t, 1H, J_2 = 7.5Hz, Ar-H), 6.80 (d, 1H, J_2 = 7.5Hz, Ar-H), 7.00 (t, 1H, J_2 = 7.2Hz, Ar-H), 7.15 (m, 2H, Ar-H), 7.29 (d, 1H, J_2 = 1.8Hz, Ar-H), 7.46–7.55 (m, 3H, Ar-H), 7.75 (m, 2H, Ar-H), 7.98 (m, 3H, Ar-H), 8.88 (s, 1H, CH), 9.19 (t, 1H, J_2 = 5.7Hz, Ar), 9.66 (s, 1H, NH); ^{13}C NMR (75 MHz, DMSO-d_6) δ 42.98, 67.78, 101.70, 113.07, 114.43, 115.79, 116.58, 116.77, 123.69, 126.93, 127.05, 127.62, 128.15, 128.36, 129.58, 129.93, 132.21, 132.44, 132.98, 133.72, 134.55, 143.11, 143.45, 148.34, 156.53, 161.21, 162.06, 163.50, 165.56; LCMS(ESI, m/z): 589.1 $[M+1]^+$; Anal. calcd. for $C_{31}H_{23}Cl_2N_3O_5$: C, 63.27; H, 3.94; N, 7.14; found: C, 63.15; H, 4.08; N, 7.25.

4.6.21. N-(4-((2-aminophenyl) carbamoyl) benzyl)-7-((3,4-dichlorobenzyl)oxy)-2-oxo-2H-chromene-3-carboxamide (**8u**)

White solid; yield: 87%; mp: 206–207 °C; R_f = 0.55 (petroleum ether: ethyl acetate = 3:2); IR (KBr): ν_{max} (cm^{-1}) 3402 and 3355 (NH and NH_2), 1701, 1654 and 1615 (CO); ^1H NMR (300 MHz, DMSO-d_6) δ 4.62 (d, 2H, J = 5.7Hz, CH_2), 4.90 (brs, 2H, NH_2), 5.30 (s, 2H, OCH_2), 6.61 (t, 1H, J = 7.2Hz, Ar-H), 6.80 (d, 1H, J = 8.1Hz, Ar-H), 7.98 (t, 1H, J = 8.1Hz, Ar-H), 7.13–7.23 (m, 3H, Ar-H), 7.70 (d, 1H, J = 8.1Hz, Ar-H), 7.80 (d, 1H, J = 1.8Hz, Ar-H), 7.93–7.97 (m, 3H, Ar-H), 8.87 (s, 1H, CH), 9.18 (t, 1H, J = 6.0Hz, NH), 9.65 (s, 1H, NH); ^{13}C NMR (75 MHz, DMSO-d_6) δ 42.98, 69.00, 101.74, 113.006, 114.47, 115.74, 116.58, 116.77, 123.68, 123.78, 126.94, 127.06, 127.61, 128.35, 128.63, 130.30, 131.30, 131.69, 132.18, 133.72, 137.70, 143.11, 143.45, 148.34, 156.51, 161.21, 162.14, 163.44, 165.52; LCMS(ESI, m/z): 588.1 $[M]^+$, 589.0 $[M+1]^+$, 1176.3 $[2\ M]^+$; Anal. calcd. for $C_{31}H_{23}Cl_2N_3O_5$: C, 63.27; H, 3.94; N, 7.14; found: C 63.40, H 4.06, N, 7.02.

4.7. Biological evaluation

4.7.1. Cell growth inhibition assay

The level of in vitro proliferative response of cancer cells and normal cells were estimated using MTT dye assay. Cancer cells and normal cells were maintained in RPMI 1640 (Gibco, USA) and in DMEM medium (Caisson, USA), respectively. After counting the number of cells with a hemocytometer by 0.04% Trypan Blue dye exclusion technique, the cells were cultured in 96-well microplates (1×10^4 cells/100 μL in each well) with RPMI 1640 or DMEM medium which were incubated for 24 h at 37 °C in 5% CO_2 incubator. Inhibitor solutions were prepared by serial dilution of a 5 mM DMSO stock solution with culture medium. The final amount of

DMSO per well was maintained at below 1% V/V. Then, the cells were treated with the different concetrations of the test compounds, positive control Entinostat and medium alone with or without 1% DMSO as negative controls for 48 h at 37 °C with 5% CO_2. Thereafter, 150 μL MTT solution diluted in culture medium (5 mg/ml) was added to each well and incubation continued for 4 h. Then, the supernatants were carefully removed and formazan precipitates were dissolved in 150 μL of DMSO. Plates were shaken vigorously (300 rpm) for 5 min. Finally, the difference of absorbance at 570 nm and 630 nm was measured with Microplate Spectrophotometer (BioTec, USA). Each assay was performed in triplicate. The inhibition percentage of test compounds with concentrations (10–100 μM) was calculated as: $\Delta OD_{\text{wells treated with compounds}}/\Delta OD_{\text{wells treated with medium alone}} \times 100$. Then, IC_{50} values were calculated by nonlinear regression analysis using GraphPad prism (Version 6.0) software and expressed in mean ± SD.

4.7.2. Whole-cell HDAC inhibition assay

Briefly, human cancer cell lines A2780 and HCT-116 were seeded in 96-well tissue culture microplates (1.5×10^4 cells/90 μL culture medium in each well). After 24 h, cells were incubated for 18 h with increasing concentrations of test compounds. The reaction was started by adding 10 μL of 3 mM Boc-Lys (ε-Ac)-AMC (Bachem, Koln, Germany) to each well at a final concentration of 0.3 mM. The cells were incubated with the Boc-Lys (ε-Ac)-AMC for 3 h under cell culture conditions. After this incubation, 100 μL/well stop solution (25 mM Tris-HCl (pH 8), 137 mM NaCl, 2.7 mM KCl, 1 mM $MgCl_2$, 1% NP40, 2.0 mg/mL trypsin, 10 μM vorinostat) was added and the mixture was developed for 3 h under cell culture conditions. Fluorescence intensity was measured at an excitation of 320 nm and emission of 520 nm in a NOVOstar microplate reader (BMG LabTech, Offenburg, Germany) [47].

4.7.3. In vitro HDAC1 inhibition fluorescence assay

The HDAC1 inhibitory activity of the four potent compounds was evaluated using commercially HDAC1 fluorescent Activity Assay Kit (Biomol, #AK511, USA) following the manufacturer manual. Briefly, HDAC1 enzyme, test compounds and substrate were diluted with HDAC assay buffer (50 mM Tris-HCl, pH 8.0, 137 mM NaCl, 2.7 mM KCl, 1 mM $MgCl_2$, 1 mg/mL BSA). 15 μL diluted HDAC1 enzyme was preincubated with 10 μL of different concetrations of the test compounds (10–100 μM) in 96-well microplates for 5 min at 30 °C. To start the reaction, deacetylase fluorogenic substrate (25 μL) was added and the reaction mixture incubated for 30 min at 30 °C. Then, the reaction was stopped by addition of 50 μL developer/TSA (trichostatin A). After 45 min incubation, the fluorescent intensity was measured by a microplate reader at excitation and emission wavelengths of 350 and 460 nm, respectively. The inhibition ratios were calculated from the fluorescence intensity readings of tested wells relative to those of control wells [51]. IC_{50} values were calculated by nonlinear regression analysis using GraphPad prism (Version 6.0) software and expressed in mean ± SD.

4.8. Molecular docking

The molecular docking process performed using AutoDock4.2 (http://autodock.scripps.edu/) to predict the best possible biological conformation of target compound in the active site of a particular protein. The x-ray crystal structure of HDAC1 (PDB ID: 4BKX) with resolution 2.5 Å was downloaded from the Protein Data Bank (PDB). Water molecules, co-crystallized ligand and all ions except the catalytic zinc ion were removed and polar hydrogen atoms were added to the receptor, then the protein was saved with pdbqt format using the graphical user interface Autodock tools (ADT, 1.5.6). The 2D structure of the target compounds was prepared using Chem Draw Ultra 8.0 software (http://www.cambridgesoft.com/) and converted to 3D format by Hyper Chem7 (Hyper cube Inc, USA) using AM1 semi-empirical method, and the pdbqt format of the target compounds was prepared using ADT. The target compounds were docked into the active pocket of HDAC1. A gridbox size of $70 \times 70 \times 70$ points with 0.375 Å spacing between the grid points was used. Gridbox center was located at center of co-crystallized ligand ($x = -47.557$, $y = 16.078$, $z = -4.771$). AutoGrid 4.2 was used to generate the grid map files for the docking calculations. Then AutoDock4.2 was run. Lamarckian Genetic Algorithm (GA) parameters were set to 100 GA runs with a population size of 150; a maximum number of 2.5×10^5 energy evaluation and 2.7×10^4 generation were used. The other parameters were set as default. The output DLG files were converted to pdb format and Molecular Operating Environment (MOE) (www.chemcomp.com) was employed to view the docking results. The best docking pose of compound **8a** was chosen for Molecular dynamic (MD) simulation.

4.9. Molecular dynamic simulation

Molecular Dynamic (MD) simulation studies were performed to investigate the interaction between the protein and ligand in atomic details at real physiological condition aqueous solution at $T = 37$ °C, $P = 1$atm. Calculations were performed using the Nanoscale Molecular Dynamics NAMD 2.9 program (www.ks.uiuc.edu/Research/namd) with CHARMM27 force field. The visualization package Visual Molecular Dynamics (VMD) (www.ks.uiuc.edu/Research/vmd) was used to analyze results. The force field parameters of the ligand **8a** were prepared by SwissParam (http://swissparam.chr). The structure of protein was checked for missing atoms and bonds the whole systems were immersed in the center of a TIPS water box with dimensions $6 \times 6 \times 6$ nm, using the VMD program and the systems were neutralized by adding sodium and chloride ions and energy minimization with the steepest descent method for 5000 steps. The Particle-Mesh Ewald (PME) algorithm with a grid spacing of 1Å and periodic boundary conditions were applied. A cut-off 15 (Å) was applied to the short-range Lennard-Jones interactions. Finally, the MD simulations were performed with a time step of 2 fs for 70 ns (ns). The trajectory of the system was stored at every 1ps and analyzed by VMD analyzer Tools.

The system was complex and required significant computational. We used resources at the National High-Performance Computing Center Isfahan University of Technology (http://nhpcc.iut.ac.ir). 32 Intel xenon processors (2.5-GHz) were employed.

4.10. Prediction of physicochemical and ADME properties

The physicochemical and ADME properties of the coumarin compounds as drug candidate were predicted using Schrödinger module QikProp 0.8 (Schrödinger, LLC, New York, 2015, USA). It is a quick, accurate and easy method for prediction of absorption, distribution, metabolism, elimination and toxicity (ADMET) properties.

Acknowledgements

We are grateful to Research deputy of Mashhad University of Medical Sciences for financial support of this research (grant no. 931419). This work was part of Ph.D thesis of T. Abdizadeh.

Appendix A. Supplementary data

Supplementary data related to this article can be found at http://dx.doi.org/10.1016/j.ejmech.2017.03.024.

References

[1] R.L. Siegel, K.D. Miller, A. Jemal, Cancer statistics, 2015, CA Cancer J. Clin. 65 (2015) 5–29.
[2] K. Nepali, S. Sharma, M. Sharma, P.M.S. Bedi, K.L. Dhar, Rational approaches, design strategies, structure activity relationship and mechanistic insights for anticancer hybrids, Eur. J. Med. Chem. 77 (2014) 422–487.
[3] X.J. Yang, E. Seto, The Rpd3/Hda1 family of lysine deacetylases: from bacteria and yeast to mice and men, Nat. Rev. Mol. Cell. Biol. 9 (2008) 206–218.
[4] C. Monneret, Histone deacetylase inhibitors, Eur. J. Med. Chem. 40 (2005) 1–13.
[5] J.E. Bolden, M.J. Peart, R.W. Johnstone, Anticancer activities of histone deacetylase inhibitors, Nat. Rev. Drug. Discov. 5 (2006) 769–784.
[6] H.Y. Lee, A.C. Tsai, M.C. Chen, P.J. Shen, Y.C. Cheng, C.C. Kuo, S.L. Pan, Y.M. Liu, J.F. Liu, T.K. Yeh, J.C. Wang, C.Y. Chang, J.Y. Chang, J.P. Liou, Azaindolylsulfonamides, with a more selective inhibitory effect on histone deacetylase 6 activity, exhibit antitumor activity in colorectal cancer HCT116 cells, J. Med. Chem. 57 (2014) 4009–4022.
[7] M. Grunstein, Histone acetylation in chromatin structure and transcription, Nature 389 (1997) 349–352.
[8] K. Struhl, Histone acetylation and transcriptional regulatory mechanisms, Genes. Dev. 12 (1998) 599–606.
[9] Y. Zhang, J. Feng, Y. Jia, Y. Xu, C. Liu, H. Fang, W. Xu, Design, synthesis and primary activity assay of tripeptidomimetics as histone deacetylase inhibitors with linear linker and branched cap group, Eur. J. Med. Chem. 46 (2011) 5387–5397.
[10] F. Wang, W. Lu, T. Zhang, J. Dong, H. Gao, P. Li, S. Wang, J. Zhang, Development of novel ferulic acid derivatives as potent histone deacetylase inhibitors, Bioorg. Med. Chem. 21 (2013) 6973–6980.
[11] W.-J. Huang, C.-C. Chen, S.-W. Chao, C.-C. Yu, C.-Y. Yang, J.-H. Guh, Y.-C. Lin, C.-I. Kuo, P. Yang, C.-I. Chang, Synthesis and evaluation of aliphatic-chain hydroxamates capped with osthole derivatives as histone deacetylase inhibitors, Eur. J. Med. Chem. 46 (2011) 4042–4049.
[12] P.A. Marks, T. Miller, V.M. Richon, Histone deacetylases, Curr. Opin. Pharmacol. 3 (2003) 344–351.
[13] A.J. de Ruijter, A.H. van Gennip, H.N. Caron, S. Kemp, A.B. van Kuilenburg, Histone deacetylases (HDACs): characterization of the classical HDAC family, Biochem. J. 370 (2003) 737–749.
[14] C. Salmi-Smail, A. Fabre, F. Dequiedt, A. Restouin, R. Castellano, S. Garbit, P. Roche, X. Morelli, J.M. Brunel, Y. Collette, Modified cap group suberoylanilide hydroxamic acid histone deacetylase inhibitor derivatives reveal improved selective antileukemic activity, J. Med. Chem. 53 (2010) 3038–3047.
[15] A. Saito, T. Yamashita, Y. Mariko, Y. Nosaka, K. Tsuchiya, T. Ando, T. Suzuki, T. Tsuruo, O. Nakanishi, A synthetic inhibitor of histone deacetylase, MS-27-275, with marked in vivo antitumor activity against human tumors, Proc. Natl. Acad. Sci. U. S. A. 96 (1999) 4592–4597.
[16] F. Thaler, C. Mercurio, Towards selective inhibition of histone deacetylase isoforms: what has been achieved, where we are and what will be next, Chem.Med. Chem. 9 (2014) 523–536.
[17] K. Huber, G. Superti-Furga, After the grape rush: sirtuins as epigenetic drug targets in neurodegenerative disorders, Bioorg. Med. Chem. 19 (2011) 3616–3624.
[18] Q.-W. Zhang, J.-Q. Li, Synthesis and biological evaluation of N-(aminopyridine) benzamide analogues as histone deacetylase inhibitors, Bull. Korean. Chem. Soc. 33 (2012) 535–540.
[19] S.D. Kattar, L.M. Surdi, A. Zabierek, J.L. Methot, R.E. Middleton, B. Hughes, A.A. Szewczak, W.K. Dahlberg, A.M. Kral, N. Ozerova, J.C. Fleming, H. Wang, P. Secrist, A. Harsch, J.E. Hamill, J.C. Cruz, C.M. Kenific, M. Chenard, T.A. Miller, S.C. Berk, P. Tempest, Parallel medicinal chemistry approaches to selective HDAC1/HDAC2 inhibitor (SHI-1:2) optimization, Bioorg. Med. Chem. Lett. 19 (2009) 1168–1172.
[20] M.K. Wambua, D.A. Nalawansha, A.T. Negmeldin, M.K. Pflum, Mutagenesis studies of the 14 A internal cavity of histone deacetylase 1: insights toward the acetate-escape hypothesis and selective inhibitor design, J. Med. Chem. 57 (2014) 642–650.
[21] D.R. Walkinshaw, X.J. Yang, Histone deacetylase inhibitors as novel anticancer therapeutics, Curr. Oncol. 15 (2008) 237–243.
[22] M. Yoshida, Potent and specific inhibition of mammalian histone deacetylase both in vivo and in vitro by trichostatin A, Tanpakushitsu. Kakusan. Koso. Protein, nucleic Acid. enzyme 52 (2007) 1788–1789.
[23] S. Grant, C. Easley, P. Kirkpatrick, Vorinostat, Nat. Rev. Drug. Discov. 6 (2007) 21–22.
[24] K.P. Garnock-Jones, Panobinostat: first global approval, Drugs 75 (2015) 695–704.
[25] H.-Z. Lee, V.E. Kwitkowski, P.L. Del Valle, M.S. Ricci, H. Saber, B.A. Habtemariam, J. Bullock, E. Bloomquist, Y.L. Shen, X.-H. Chen, FDA approval: belinostat for the treatment of patients with relapsed or refractory peripheral T-cell lymphoma, Clin. Cancer. Res. 21 (2015) 2666–2670.
[26] T. Suzuki, T. Ando, K. Tsuchiya, N. Fukazawa, A. Saito, Y. Mariko, T. Yamashita, O. Nakanishi, Synthesis and histone deacetylase inhibitory activity of new benzamide derivatives, J. Med. Chem. 42 (1999) 3001–3003.
[27] S. Balasubramanian, E. Verner, J.J. Buggy, Isoform-specific histone deacetylase inhibitors: the next step? Cancer. Lett. 280 (2009) 211–221.
[28] M. Fournel, C. Bonfils, Y. Hou, P.T. Yan, M.C. Trachy-Bourget, A. Kalita, J. Liu, A.H. Lu, N.Z. Zhou, M.F. Robert, J. Gillespie, J.J. Wang, H. Ste-Croix, J. Rahil, S. Lefebvre, O. Moradei, D. Delorme, A.R. Macleod, J.M. Besterman, Z. Li, MGCD0103, a novel isotype-selective histone deacetylase inhibitor, has broad spectrum antitumor activity in vitro and in vivo, Mol. Cancer. Ther. 7 (2008) 759–768.
[29] O. Moradei, A. Vaisburg, R.E. Martell, Histone deacetylase inhibitors in cancer therapy: new compounds and clinical update of benzamide-type agents, Curr. Top. Med. Chem. 8 (2008) 841–858.
[30] L.K. Gediya, A. Belosay, A. Khandelwal, P. Purushottamachar, V.C.O. Njar, Improved synthesis of histone deacetylase inhibitors (HDIs) (MS-275 and CI-994) and inhibitory effects of HDIs alone or in combination with RAMBAs or retinoids on growth of human LNCaP prostate cancer cells and tumor xenografts, Bioorg. Med. Chem. 16 (2008) 3352–3360.
[31] N. Khan, M. Jeffers, S. Kumar, C. Hackett, F. Boldog, N. Khramtsov, X. Qian, E. Mills, S.C. Berghs, N. Carey, P.W. Finn, L.S. Collins, A. Tumber, J.W. Ritchie, P.B. Jensen, H.S. Lichenstein, M. Sehested, Determination of the class and isoform selectivity of small-molecule histone deacetylase inhibitors, Biochem. J. 409 (2008) 581–589.
[32] S. Chateauvieux, F. Morceau, M. Dicato, M. Diederich, Molecular and therapeutic potential and toxicity of valproic acid, J. Biomed. Biotechnol. 2010 (2010).
[33] R. Furumai, A. Matsuyama, N. Kobashi, K.H. Lee, M. Nishiyama, H. Nakajima, A. Tanaka, Y. Komatsu, N. Nishino, M. Yoshida, S. Horinouchi, FK228 (depsipeptide) as a natural prodrug that inhibits class I histone deacetylases, Cancer. Res. 62 (2002) 4916–4921.
[34] R. Liu, J. Wang, W. Tang, H. Fang, Design and synthesis of a new generation of substituted purine hydroxamate analogs as histone deacetylase inhibitors, Bioorg. Med. Chem. 24 (2016) 1446–1454.
[35] J. Cai, H. Wei, K.H. Hong, X. Wu, M. Cao, X. Zong, L. Li, C. Sun, J. Chen, M. Ji, Discovery and preliminary evaluation of 2-aminobenzamide and hydroxamate derivatives containing 1,2,4-oxadiazole moiety as potent histone deacetylase inhibitors, Eur. J. Med. Chem. 96 (2015) 1–13.
[36] M.S. Finnin, J.R. Donigian, A. Cohen, V.M. Richon, R.A. Rifkind, P.A. Marks, R. Breslow, N.P. Pavletich, Structures of a histone deacetylase homologue bound to the TSA and SAHA inhibitors, Nature 401 (1999) 188–193.
[37] P. Bertrand, Inside HDAC with HDAC inhibitors, Eur. J. Med. Chem. 45 (2010) 2095–2116.
[38] C. Seidel, M. Schnekenburger, C. Zwergel, F. Gaascht, A. Mai, M. Dicato, G. Kirsch, S. Valente, M. Diederich, Novel inhibitors of human histone deacetylases: design, synthesis and bioactivity of 3-alkenoylcoumarines, Bioorg. Med. Chem. Lett. 24 (2014) 3797–3801.
[39] M.E. Riveiro, A. Moglioni, R. Vazquez, N. Gomez, G. Facorro, L. Piehl, E.R. de Celis, C. Shayo, C. Davio, Structural insights into hydroxycoumarin-induced apoptosis in U-937 cells, Bioorg. Med. Chem. 16 (2008) 2665–2675.
[40] Y. Shikishima, Y. Takaishi, G. Honda, M. Ito, Y. Takfda, O.K. Kodzhimatov, O. Ashurmetov, K.H. Lee, Chemical constituents of Prangos tschiniganica; structure elucidation and absolute configuration of coumarin and furanocoumarin derivatives with anti-HIV activity, Chem. Pharm. Bull. 49 (2001) 877–880.
[41] A. Asadipour, M. Alipour, M. Jafari, M. Khoobi, S. Emami, H. Nadri, A. Sakhteman, A. Moradi, V. Sheibani, F. Homayouni Moghadam, A. Shafiee, A. Foroumadi, Novel coumarin-3-carboxamides bearing N-benzylpiperidine moiety as potent acetylcholinesterase inhibitors, Eur. J. Med. Chem. 70 (2013) 623–630.
[42] D.A. Ostrov, J.A. Hernandez Prada, P.E. Corsino, K.A. Finton, N. Le, T.C. Rowe, Discovery of novel DNA gyrase inhibitors by high-throughput virtual screening, Antimicrob. Agents. Chemother. 51 (2007) 3688–3698.
[43] I. Kostova, S. Bhatia, P. Grigorov, S. Balkansky, V. S Parmar, A. K Prasad, L. Saso, Coumarins as antioxidants, Curr. Med. Chem. 18 (2011) 3929–3951.
[44] F.E. Massimo Curini, Federica Maltese, Maria Carla Marcotullio, Sylvia Prieto Gonzales, Juan Carlos, Rodriguez Synthesis of collinin, an antiviral coumarin, Aust. J. Chem. 56 (2003) 59–60.
[45] J. Dandriyal, R. Singla, M. Kumar, V. Jaitak, Recent developments of C-4 substituted coumarin derivatives as anticancer agents, Eur. J. Med. Chem. 119 (2016) 141–168.
[46] Q. Sun, D.-Y. Peng, S.-G. Yang, X.-L. Zhu, W.-C. Yang, G.-F. Yang, Syntheses of coumarin–tacrine hybrids as dual-site acetylcholinesterase inhibitors and their activity against butylcholinesterase, Aβ aggregation, and β-secretase, Bioorg. Med. Chem. 22 (2014) 4784–4791.
[47] L. Marek, A. Hamacher, F.K. Hansen, K. Kuna, H. Gohlke, M.U. Kassack, T. Kurz, Histone deacetylase (HDAC) inhibitors with a novel connecting unit linker region reveal a selectivity profile for HDAC4 and HDAC5 with improved activity against chemoresistant cancer cells, J. Med. Chem. 56 (2013) 427–436.
[48] P.Y. Muller, M.N. Milton, The determination and interpretation of the therapeutic index in drug development, Nat. Rev. Drug. Discov. 11 (2012) 751–761.

[49] S. Shinde, M. Mol, V. Jamdar, S. Singh, Molecular modeling and molecular dynamics simulations of GPI 14 in Leishmania major: insight into the catalytic site for active site directed drug design, J. Theor. Biol. 351 (2014) 37–46.
[50] A.C. Wallace, R.A. Laskowski, J.M. Thornton, LIGPLOT: a program to generate schematic diagrams of protein-ligand interactions, Protein. Eng. 8 (1995) 127–134.
[51] Y. Zhang, J. Feng, Y. Jia, X. Wang, L. Zhang, C. Liu, H. Fang, W. Xu, Development of tetrahydroisoquinoline-based hydroxamic acid derivatives: potent histone deacetylase inhibitors with marked in vitro and in vivo antitumor activities, J. Med. Chem. 54 (2011) 2823–2838.